

Non-separable covariance models for spatio-temporal data, with applications to neural encoding analysis*

Seyoung Park*, Kerby Shedden[†] and Shuheng Zhou[†]

*School of Public Health, Yale University**

e-mail: seyoung.park@yale.edu

University of Michigan^{††}

e-mail: kshedden@umich.edu e-mail: shuhengz@umich.edu

Abstract: Neural encoding studies explore the relationships between measurements of neural activity and measurements of a behavior that is viewed as a response to that activity. The coupling between neural and behavioral measurements is typically imperfect and difficult to measure. To enhance our ability to understand neural encoding relationships, we propose that a behavioral measurement may be decomposable as a sum of two latent components, such that the direct neural influence and prediction is primarily localized to the component which encodes temporal dependence. For this purpose, we propose to use a non-separable Kronecker sum covariance model to characterize the behavioral data as the sum of terms with exclusively trial-wise, and exclusively temporal dependencies. We then utilize a corrected form of Lasso regression in combination with the nodewise regression approach for estimating the conditional independence relationships between and among variables for each component of the behavioral data, where normality is necessarily assumed. We provide the rate of convergence for estimating the precision matrices associated with the temporal as well as spatial components in the Kronecker sum model. We illustrate our methods and theory using simulated data, and data from a neural encoding study of hawkmoth flight; we demonstrate that the neural encoding signal for hawkmoth wing strokes is primarily localized to a latent component with temporal dependence, which is partially obscured by a second component with trial-wise dependencies.

Keywords and phrases: Kronecker sum, errors-in-variables regression, space-time covariance model, neural data analysis.

*The research is supported by DMS-13-16731, and the Elizabeth Caroline Crosby Research Award to SZ from the University of Michigan.

1. Introduction

Statistics, machine learning and a broad range of application areas such as genomics, neuroscience, and spatio-temporal modeling (Smith et al., 2003; Bonilla et al., 2008; Werner et al., 2008; Yu et al., 2009; Kalaitzis et al., 2013) that heavily rely on large-scale automated data analysis are sparking one another's development in recent years. In this setting, an important role for statistics is to provide models that can accommodate the science and design computational efficient methods for dealing with large, complex and high dimensional data arise from these application domains.

Neuroscience experiments often involve a large number of trials over varying experimental conditions, often on only a modest number of subjects. In an experimental setting, Sponberg et al. (2015) are able to directly measure neural activity and motion characteristics of hawkmoths, which are known to be agile flyers whose flights are controlled by their complex neural systems. Motor control is a complex process that involves the coordination of many muscles to produce a complex movement. Animal flight is an especially intricate type of motion that is produced by wing strokes that take place at high temporal frequency. Studying neurocontrol of flight therefore involves a regression relationship between measurements of neural activity and measurements of motion which are high-frequency, high-dimensional, and affected by substantial measurement error.

We first review the errors-in-variables (EIV) regression model with dependent measurements as studied in Rudelson and Zhou (2017). Suppose that we observe $y \in \mathbb{R}^n$ and $X \in \mathbb{R}^{n \times m}$ in the following regression model

$$y = X_0 \beta^* + \varepsilon, \quad \text{where} \quad X = X_0 + W, \quad (1)$$

where $\beta^* \in \mathbb{R}^m$ is an unknown vector to be estimated, X_0 is an $n \times m$ design matrix and W is a mean zero $n \times m$ random noise matrix, independent of X_0 and ε , whose columns are also independent and each consists of dependent elements. That is, we consider $\mathbb{E} \omega^j \otimes \omega^j = B$ for all $j = 1, \dots, m$, where ω^j denotes the j^{th} column vector of W . Here \otimes denotes the Kronecker Product. Here we assume that the noise vector $\varepsilon \in \mathbb{R}^n$ is independent of W or X_0 , with independent entries ε_j satisfying $\mathbb{E}[\varepsilon_j] = 0$ and $\|\varepsilon_j\|_{\psi_2} \leq M_\varepsilon$, where recall the ψ_2 condition on a scalar random variable V is equivalent to the subgaussian tail decay of V , which means $\mathbb{P}(|V| > t) \leq 2 \exp(-t^2/c^2)$, for all $t > 0$ for some constant c .

Using data from a study of [Sponberg et al. \(2015\)](#), we show that the hawkmoth flight motion data can be decomposed additively into two components X_0 and W , (cf. (3)), where X_0 contains most of the temporal correlation that is related to neural firing time difference Δ , and W is minimally related to neural activity and therefore can be viewed as noise in this setting; moreover, our covariance model allows dependencies among trials to be explicitly modeled, which is significantly different from those measurement error models analyzed in the literature. This novel additive model allows the spatio-temporal features in observation data X to be parsimoniously specified, in the sense that its covariance on $\text{vec}\{X\}$ can be succinctly written as the Kronecker sum as in (3). For an $n \times m$ matrix X , $\text{vec}\{X\}$ is obtained by stacking the columns of the matrix X into a vector in \mathbb{R}^{mn} .

1.1. Models and methods

We begin with a model considered in [Rudelson and Zhou \(2017\)](#). Denote by Z a subgaussian random ensemble where Z_{ij} are independent subgaussian random variables such that

$$\mathbb{E}[Z_{ij}] = 0 \quad \text{and} \quad \|Z_{ij}\|_{\psi_2} \leq K, \quad \text{for all } i, j \quad (2)$$

for some finite constant K . Let Z_1, Z_2 be independent copies of the subgaussian random matrix Z as in (2). Assume that the random matrix X in (1) satisfies

$$X = Z_1 A^{1/2} + B^{1/2} Z_2 \sim \mathcal{M}_{n,m}(0, A \oplus B) \quad (3)$$

$$\text{where } A \oplus B := A \otimes I_n + I_m \otimes B$$

denotes the Kronecker sum of positive definite $A \in \mathbb{R}^{m \times m}$ and $B \in \mathbb{R}^{n \times n}$. We use $X \sim \mathcal{M}_{n,m}(0, A \oplus B)$ to denote the subgaussian random matrix $X_{n \times m}$ which is generated using (3) with Z_1, Z_2 being independent copies of Z as in (2). When $Z_{i,jk} \sim \mathcal{N}(0, 1)$ for all $i = 1, 2$ and all j, k , we use $X \sim \mathcal{N}_{n,m}(0, A \oplus B)$, which is equivalent to say that the n by m random matrix X follows $\text{vec}\{X\} \sim \mathcal{N}(0, A \oplus B)$. In this covariance model, the first component, $A \otimes I_n$, describes the covariance of the *signal* $X_0 = Z_1 A^{1/2}$, which is an $n \times m$ random design matrix with independent subgaussian row vectors, and the other component, $I_m \otimes B$, describes the covariance for the *noise matrix* $W = B^{1/2} Z_2$, which contains independent subgaussian column vectors w^1, \dots, w^m , independent of X_0 . This leads to a non-separable class of models for the observation X .

Suppose that $\widehat{\text{tr}}(B)$ is an estimator for $\text{tr}(B)$; for example, as constructed in (9) for a single copy of data X as in (3). Let

$$\widehat{\Gamma} = \frac{1}{n}X^T X - \frac{1}{n}\widehat{\text{tr}}(B)I_m \quad \text{and} \quad \widehat{\gamma} = \frac{1}{n}X^T y. \quad (4)$$

For chosen parameters λ and b_1 , we exploit the following regularized estimation with the ℓ_1 -norm penalty to estimate β^* (Rudelson and Zhou (2017)):

$$\widehat{\beta} = \arg \min_{\beta: \|\beta\|_1 \leq b_1} \frac{1}{2}\beta^T \widehat{\Gamma} \beta - \langle \widehat{\gamma}, \beta \rangle + \lambda \|\beta\|_1. \quad (5)$$

where b_1 is understood be chosen so that $\|\beta^*\|_1 = \sum_{j=1}^m |\beta_j^*| \leq b_1$. For replicated data, we can use replicates to obtain an estimator \widehat{B} for covariance B , using methods to be described in Subsection 3.1. Then we can compute the trace of \widehat{B} and denote that by $\widehat{\text{tr}}(B) = \text{tr}(\widehat{B})$. The non-convex optimization function in (5) can be solved efficiently using the composite gradient descent algorithm; see Agarwal et al. (2012), Loh and Wainwright (2012), and Rudelson and Zhou (2017) for details. An estimator similar to (5) was considered by Loh and Wainwright (2012), which is a variation of the Lasso (Tibshirani, 1996) or the Basis Pursuit (Chen et al., 1998) estimator. For the related Conic programming estimators (and related Dantzig selector-type) for estimating β^* in (1), see Rosenbaum and Tsybakov (2010, 2013), Belloni et al. (2016), and Rudelson and Zhou (2017).

We are interested in studying the estimating the inverse covariance for A and B , which we will describe in Section 2. In Section 2, the corrected Lasso estimator will be used in the nodewise regression procedure to estimate the concentration matrices $\Theta = A^{-1}$ and $\Omega = B^{-1}$. We first focus on estimating the structures by using the nodewise regression-based approach as in Meinshausen and Bühlmann (2006). We then apply the refit procedure as in Yuan (2010) and Loh and Wainwright (2012) to obtain the final estimates of Θ and Ω . In our numerical examples, the estimated concentration matrices are subject to a suitable level of thresholding (Zhou et al., 2011).

1.2. Data analysis

The ability of flying animals to turn while in flight is controlled by the firing of neurons located in the left and right dorsolongitudinal muscles (DLMs). Recently, Sponberg and Daniel (2012) and Sponberg et al. (2015) conducted exper-

iments and developed an analytic approach to better understand this neural-motor control mechanism. In these studies, torque profiles were obtained for individual wing strokes of hawkmoths (a large bird-like moth). The torque profiles were sampled at high frequency, yielding around 500 measurements per wing stroke. The spike times of neuronal firing for the left DLM (t_L) and right DLM (t_R) were also measured for each wing stroke.

These spike times represent the time at which neuronal firing occurred immediately prior to each wing stroke. There is one pair of (t_L, t_R) measurements per wing stroke and 298-928 wing strokes are recorded for each moth. It is generally accepted that $t_L \approx t_R$ during straight flight and $t_L < t_R$ or $t_L > t_R$ when the moth makes a left or a right turn respectively. The measured difference in DLM firing $\Delta = t_L - t_R$ may be taken as a summary measure of the neural signal for turning. The observed torque profile reflects the actual turning behavior during one wing stroke. While this profile can be summarized through a simple measure such as the average torque, it is not clear what features of the torque profile are most tightly linked to the neural signal represented by Δ , and therefore may be presumed to be most directly under neural control.

[Sponberg et al. \(2015\)](#) aim to capture the variation in movement that relates to the neural signals. They apply the partial least squares (PLS) to extract the encoded features of movement based on the cross-covariance of neural signals (t_L, t_R) and torque profiles. They exploit the extracted motor features to test whether neural signals act as a synergy or independently encode information about movement.

In the present work, we focus on the Kronecker sum model to encode the covariance structure for data matrix X collected from each single moth. We allow dependencies between and among wing strokes (that is, repeated experiments under varying conditions) to be explicitly specified through the covariance matrix $B \succ 0$ in (3) while covariance matrix $A \succ 0$ is used to model the temporal dependencies among time points within each wing stroke, much like the classical time series analysis. The relative contributions of the “signal” and “noise” components vary by moth, perhaps due to inhomogeneities in the experimental conditions. Taking a purely data-driven approach, the neural encoding of motion can therefore be studied through the regression relationship between quantitative measures of neural activity in $\Delta = t_L - t_R$ (as y) and quantitative measures of motion which correspond to wing stroke data in X_0 using the model (1).

1.3. Contributions

In the proposed research, we aim to study a general class of matrix decomposition and regression problems, where the design matrix X_0 and the random error W may possess dynamic and complex dependency structures. The presence of spatially correlated noise in W across different flights motivates the consideration of errors-in-variables regression through the regression function (1) in combination with the Kronecker sum covariance model for X . Spatial dependencies in X are understood to encode correlations between and among different trials of wing strokes, which are present possibly due to the correlated measurement errors and experimental conditions. After accounting for this measurement error, the relationship between neural activity and motion is shown to be stronger.

The rest of this paper is organized as follows. In Section 2, we describe our methods for estimating the concentration matrices. In Section 3, we establish statistical convergence properties for the inverse covariance estimation problem for the matrix-variate normal distribution with Kronecker sum covariance model. In Section 4, we present simulation study which show that our proposed methods indeed achieve consistent estimation of Θ and Ω in the operator norm. In Section 5, we apply the Kronecker sum covariance model and its related errors-in-variables regression method to analyze the hawkmoth neural encoding data. We also describe the estimated Θ and Ω which encode conditional independence relationships between time points, as well as among wing strokes. In Section 6, we conclude.

Notation. For a matrix $A = (a_{ij})_{1 \leq i, j \leq m}$, we use $\|A\|_2$ to denote its operator norm and let $\|A\|_{\max} = \max_{i,j} |a_{ij}|$ denote the entry-wise max norm. Let $\|A\|_1 = \max_j \sum_{i=1}^m |a_{ij}|$ denote the matrix ℓ_1 norm. The Frobenius norm is $\|A\|_F^2 = \sum_i \sum_j a_{ij}^2$. For a square matrix A , let $\text{tr}(A)$ be the trace of A , $\text{diag}(A)$ be a diagonal matrix with the same diagonal as A , and $\kappa(\Sigma)$ denote the condition number of A . Let I_n be the n by n identity matrix. For two numbers a, b , $a \wedge b := \min(a, b)$ and $a \vee b := \max(a, b)$. For a function $g : \mathbb{R}^m \rightarrow \mathbb{R}$, we write ∇g to denote a gradient or subgradient, if it exists. Let $(a)_+ := a \vee 0$. We use $a = O(b)$ or $b = \Omega(a)$ if $a \leq Cb$ for some positive absolute constant C which is independent of n, m or sparsity parameters. We write $a \asymp b$ if $ca \leq b \leq Ca$ for some positive absolute constants c, C . The absolute constants C, C_1, c, c_1, \dots

may change line by line. We list a set of symbols we use throughout the paper in Table 4 at the end of the paper.

2. The additive Gaussian graphical models

Consider (3) where we assume Z_1 and Z_2 are independent copies of a Gaussian random ensemble Z , where $Z_{ij} \sim \mathcal{N}(0, 1)$ for all i, j . The results in Rudelson and Zhou (2017) naturally lead to the following considerations for estimating the precision matrix $\Theta := A^{-1}$. Similarly, we obtain $\hat{\Omega}$, the estimator for precision matrix $\Omega = B^{-1}$.

Estimating Θ via Nodewise Regression To construct an estimator for $\Theta = A^{-1}$ with $X = X_0 + W$ as defined in (3), we obtain m vectors of $\hat{\beta}^i, i = 1, \dots, m$, by solving (5) with $\hat{\Gamma}$ and $\hat{\gamma}$ set to be

$$\hat{\Gamma}^{(i)} = \frac{1}{n} X_{-i}^T X_{-i} - \hat{\tau}_B I_{m-1} \quad \text{and} \quad \hat{\gamma}^{(i)} = \frac{1}{n} X_{-i}^T X_i \quad (6)$$

where X_{-i} denotes columns of X without i and $\hat{\tau}_B$ is an estimator for $\tau_B = \text{tr}(B)/n$. For a chosen penalization parameter $\lambda \geq 0$ and a fixed $b_1 > 0$, consider the following variant of the Lasso estimator

$$\hat{\beta}^i = \arg \min_{\beta \in \mathbb{R}^{m-1}, \|\beta\|_1 \leq b_1} \left\{ \frac{1}{2} \beta^T \hat{\Gamma}^{(i)} \beta - \langle \hat{\gamma}^{(i)}, \beta \rangle + \lambda \|\beta\|_1 \right\}. \quad (7)$$

Covariance estimation can be obtained through procedures which involve calculating variances for the residual errors after obtaining regression coefficients or through the MLE refit procedure based on the associated edge set (cf. Yuan, 2010; Zhou et al., 2011). The choice of b_1 in (5) will depend on the model class for Θ , which will be chosen to provide an upper bound on the matrix ℓ_1 norm $\|\Theta\|_1$. More precisely, we can set $b_1 \asymp \max_j (\theta_{jj} \sum_{i \neq j}^m |\theta_{ij}|) \leq M \|\Theta\|_1$, assuming that $\theta_{jj} \leq M$ for some absolute constant M .

To solve the non-convex optimization problem (7), we use the composite gradient descent algorithm as studied in Agarwal et al. (2012) and Loh and Wainwright (2012). Let $L(\beta) := \frac{1}{2} \beta^T \hat{\Gamma}^{(i)} \beta - \langle \hat{\gamma}^{(i)}, \beta \rangle$. The gradient of the loss function is $\nabla L(\beta) = \hat{\Gamma}^{(i)} \beta - \hat{\gamma}^{(i)}$. The composite gradient descent algorithm produces a sequence of iterates $\{\beta^{(t)}, t = 0, 1, 2, \dots\}$ by

$$\beta^{(t+1)} = \arg \min_{\|\beta\|_1 \leq b_1} L(\beta^{(t)}) + \langle \nabla L(\beta^{(t)}), \beta - \beta^{(t)} \rangle + \frac{\eta}{2} \|\beta - \beta^{(t)}\|_2^2 + \lambda \|\beta\|_1 \quad (8)$$

with the step size parameter $\eta > 0$.

For the Kronecker sum model as in (1) and (3) to be identifiable, we assume the trace of A is known.

(A1) We assume $\text{tr}(A) = m$ is a known parameter.

For example, any m -dimensional correlation matrix satisfies (A1). We defer the discussion on condition (A1) in Section 2.1. For a model where replicated measurements of X_0 are available, we do not need to assume that (A1) holds. Assuming $\text{tr}(A)$ or $\text{tr}(B)$ is known is unavoidable as the covariance model is not identifiable otherwise for a single sample case. By knowing $\text{tr}(A)$, we can construct an estimator for $\text{tr}(B)$ following Rudelson and Zhou (2017),

$$\widehat{\text{tr}}(B) := \frac{1}{m} (\|X\|_F^2 - n \text{tr}(A))_+ \quad \text{and} \quad \widehat{\tau}_B := \frac{1}{n} \widehat{\text{tr}}(B). \quad (9)$$

Let $Z_1 = (Z_{1,ij})_{n \times m}$ be a Gaussian random ensemble with independent standard normal entries. To estimate the precision matrix Θ , first consider the following regressions, where we regress one variable against all others: for $X_0 = Z_1 A^{1/2}$ defined in (3), the j th column of X_0 satisfies

$$X_{0,j} = X_{0,-j} \beta^j + V_{0,j}, \quad (10)$$

$$\text{where } V_{0,j} \sim \mathcal{N}(0_n, \sigma_{V_j}^2 I_n) \text{ is independent of } X_{0,-j}, \quad (11)$$

where $X_{0,j}$ denotes the j th column of X_0 , $X_{0,-j}$ denotes the matrix of X_0 with its j th column removed, $\sigma_{V_j}^2 := A_{jj} - A_{j,-j} A_{-j,-j}^{-1} A_{-j,j}$, and $\beta^j \in \mathbb{R}^{m-1}$ corresponds to a vector of regression coefficients. One can verify that

$$\Theta_{jj} = (A_{jj} - A_{j,-j} \beta^j)^{-1} \quad \text{and} \quad \Theta_{j,-j} = -(A_{jj} - A_{j,-j} \beta^j)^{-1} \beta^j. \quad (12)$$

Now the j^{th} column of X in (1) can be written as

$$X_j = X_{0,-j} \beta^j + V_{0,j} + W_j =: X_{0,-j} \beta^j + \varepsilon_j, \quad j = 1, \dots, m,$$

where we observe $X_{-j} = X_{0,-j} + W_{-j}$, which resembles (1).

The noise $\varepsilon_j = V_{0,j} + W_j$ is independent of $\{X_i; i \neq j\}$ ($i = 1, \dots, m$), but the components of ε_j are correlated due to W_j . Thus this fits in the errors-in-variables framework despite the complication due to the dependence within components of ε_j for all j . We estimate β^i for each i with (7) and then obtain Θ by using (12). We summarize the algorithm as follows:

Algorithm 1: Input $(\hat{\Gamma}^{(j)}, \hat{\gamma}^{(j)})$ as in (6) and $\hat{\Gamma}$ as in (4)

- (1) Perform m regressions using (7) to obtain vectors of $\hat{\beta}^j \in \mathbb{R}^{m-1}$, $j = 1, \dots, m$, with penalization parameters $\lambda^{(j)}, b_1 > 0$ to be specified.
- (2) Construct $\tilde{\Theta} \in \mathbb{R}^{m \times m}$ in view of (12), such that for $j = 1, \dots, m$,

$$\tilde{\Theta}_{j,-j} = -(\hat{\Gamma}_{jj} - \hat{\Gamma}_{j,-j}\hat{\beta}^j)^{-1}\hat{\beta}^j, \text{ and } \tilde{\Theta}_{jj} = (\hat{\Gamma}_{jj} - \hat{\Gamma}_{j,-j}\hat{\beta}^j)^{-1}.$$

- (3) Project $\tilde{\Theta}$ onto the space \mathcal{S}^m of $m \times m$ symmetric matrices:

$$\hat{\Theta} = \arg \min_{\Theta \in \mathcal{S}^m} \left\| \Sigma - \tilde{\Theta} \right\|_1.$$

Our theoretical results show that this procedure indeed achieves consistent estimation of Θ in the operator norm under suitable assumptions.

2.1. Related work

For matrix-variate data with two-way dependencies, prior work depended on a large number of replicated data to obtain certain convergence guarantees, even when the data is observed in full and free of measurement error; see for example Dutilleul (1999), Werner et al. (2008), Leng and Tang (2012), and Tsiligkaridis et al. (2013). A recent line of work on matrix variate models (Kalaitzis et al., 2013; Zhou, 2014; Rudelson and Zhou, 2017) have focused on the design of estimators and efficient algorithms while establishing theoretical properties by using the Kronecker sum and product covariance models when a single or a small number of replicates are available from such matrix-variate distributions; See also Efron (2009), Allen and Tibshirani (2010), and Hornstein et al. (2016) for related models and applications. Among these models, the Kronecker sum provides a covariance or precision matrix which is sparser than the Kronecker product (inverse) covariance model.

Variants of the linear errors-in-variables models in the high dimensional setting has been considered in recent work (Rosenbaum and Tsybakov, 2010; Loh and Wainwright, 2012; Rosenbaum and Tsybakov, 2013; Belloni et al., 2016; Chen and Caramanis, 2013; Sørensen et al., 2015), where oblivion in the covariance structure for row or columns of W , and a general dependency condition in the single data matrix X are not simultaneously allowed. The second key difference between our framework and the existing work is that we assume that only one observation matrix X with the single measurement error matrix W

is available. Assuming (A1) allows us to estimate $\mathbb{E}W^TW$ as required in the estimation procedure (4) directly, given the knowledge that W is composed of independent column vectors. In contrast, existing work needs to assume that the covariance matrix $\Sigma_W := \frac{1}{n}\mathbb{E}W^TW$ of the independent row vectors of W or its functionals are either known a priori, or can be estimated from a dataset independent of X , or from replicated X measuring the same X_0 ; see for example Carroll et al. (2006), Rosenbaum and Tsybakov (2010), Loh and Wainwright (2012), Rosenbaum and Tsybakov (2013), and Belloni et al. (2016). Although the model we consider is different from those in the literature, the identifiability issue, which arises from the fact that we observe the data under an additive error model, is common. Such repeated measurements are not always available or costly to obtain in practice (Carroll et al., 2006). We will explore such tradeoffs in future work.

3. Theoretical properties

We require the following assumptions.

- (A2) The minimal eigenvalue $\lambda_{\min}(A)$ of the covariance matrix A is bounded:
 $1 \geq \lambda_{\min}(A) > 0$.
- (A3) The condition number $\kappa(A)$ is upper bounded by $O\left(\sqrt{\frac{n}{\log m}}\right)$ and $\tau_B = O(\lambda_{\max}(A))$.
- (A4) The covariance matrix B satisfies

$$\frac{\|B\|_F^2}{\|B\|_2^2} = \Omega(\log m), \quad \frac{\text{tr}(B)}{\|B\|_2} = \Omega\left(\frac{n}{\log m} \log \frac{m \log m}{n}\right).$$

Theorem 1 shows the statistical consistency of $\hat{\Theta}$ in the operator norm. See Table 4 for the notations used in the theorem. Proof of the theorem can be found in Section B.

Theorem 1. *Suppose conditions (A1)-(A4). Suppose the columns of Θ is d -sparse, i.e., the number of nonzero entries on each column in Θ is bounded by d , which satisfies $d = O(n/\log m)$. Suppose the condition number $\kappa(\Theta)$ is finite. Let $\hat{\beta}^i$ be an optimal solution to the nodewise regression with $b_1 := b_0\sqrt{d}$, where b_0 satisfies $\phi b_0^2 \leq \|\beta^i\|_2^2 \leq b_0^2$ for some $0 < \phi < 1$, and $D'_0 = \|B\|_2^{1/2} + a_{\max}^{1/2}$ and*

$$\lambda^{(i)} \geq \psi_i \sqrt{\frac{\log m}{n}} \quad \text{where} \quad \psi_i := C_0 D'_0 K^2 \left(\tau_B^{+/2} \|\beta^i\|_2 + \sigma_{V_i} \right) \quad (13)$$

for some positive absolute constant C_0 , where $\sigma_{V_i}^2 := A_{ii} - A_{i,-i}A_{-i,-i}^{-1}A_{-i,i}$. Then,

$$\|\hat{\Theta} - \Theta\|_2 = O_P \left(\frac{dK^2(A)}{\lambda_{\min}^2(A)} \max_i \lambda^{(i)} \right). \quad (14)$$

Moreover, suppose that $\tau_B \leq \|B\|_2 = O(\lambda_{\max}(A))$ and $\lambda^{(i)} \asymp \psi_i \sqrt{\frac{\log m}{n}}$ for each i . Then

$$\frac{\|\hat{\Theta} - \Theta\|_2}{\|\Theta\|_2} = O_P \left(\frac{K^4(A)}{\lambda_{\min}(A)} \sqrt{\frac{d \log m}{n}} \right). \quad (15)$$

Using the similar argument, we can show consistency results of $\Omega = B^{-1}$. See Theorem 4 of the Supplementary materials for details.

Remark 1. In (13), since $\beta^i = -(A_{ii} - A_{i,-i}A_{-i,-i}^{-1}A_{-i,i})\Theta_{-i,i}$,

$$\|\beta^i\|_2 \leq a_{\max} \|\Theta_{-i,i}\|_2 \leq a_{\max} \lambda_{\max}(\Theta) = \frac{a_{\max}}{\lambda_{\min}(A)},$$

where $a_{\max} := \max_i A_{ii} \geq 1$ by (A1). Together with $\sigma_{V_i}^2 \leq a_{\max}$ and $\tau_B^{+/2} = O(\sqrt{\tau_B})$, it holds that

$$\begin{aligned} \max_i \psi_i &\asymp \left(\|B\|_2^{1/2} + a_{\max}^{1/2} \right) \left(\sqrt{\tau_B} \frac{a_{\max}}{\lambda_{\min}(A)} + a_{\max}^{1/2} \right) \\ &\leq \kappa(A) (2\|B\|_2 + \tau_B + 2a_{\max}) \\ \text{thus } \frac{1}{\lambda_{\min}^2(A)} \max_i \psi_i &\leq \frac{\kappa(A)}{\lambda_{\min}(A)} \left(\frac{3\|B\|_2}{\lambda_{\min}(A)} + 2\kappa(A) \right) \asymp \frac{\kappa^2(A)}{\lambda_{\min}(A)} \end{aligned}$$

so long as $\|B\|_2 = O(\lambda_{\max}(A))$. This calculation shows that so long as $\tau_B \leq \|B\|_2 = O(\lambda_{\max}(A))$ and $\lambda^{(i)} \asymp \psi_i \sqrt{\frac{\log m}{n}}$, (15) holds. When the noise in W is negligible in the sense that τ_B (and hence $\|B\|_2$ in view of (A4)) is close to zero, then (14) reduces to

$$\|\hat{\Theta} - \Theta\|_2 = O_P \left(K^4(A) d \sqrt{\frac{\log m}{n}} \right).$$

The bound (14) is analogous to that of Corollary 5 in Loh and Wainwright (2012), where the measurement error W has independent row vectors with a known $\Sigma_W := \frac{1}{n} \mathbb{E} W^T W$.

Remark 2. Our theoretical results show that $\hat{\Theta}$ consistently estimates Θ in the spectral norm under suitable conditions. However, $\hat{\Theta}$ is not necessarily positive-semidefinite. One can obtain a consistent and positive-semidefinite estimator by considering an additional estimation procedure, which is described in Section A.

3.1. Using replicates

In the current work, we focus a class of generative models which rely on the sum of Kronecker product covariance matrices to model complex trial-wise dependencies as well as to provide a general statistical framework for dealing with signal and noise decomposition. It can be challenging to handle this type of data because there are often inhomogeneities and dependencies among the trials, and thus they can not be treated as independent replicates. In the present work, we propose a framework for explicitly modeling the variation in a set of “replicates” that may be neither independent nor identical. We denote the number of subjects by n , the number of time points by m , and the number of (non-i.i.d.) replicates by N . Let $A \in \mathbb{R}^{m \times m}$, $B, C \in \mathbb{R}^{n \times n}$ be m by m and n by n positive definite matrices, respectively. We consider the following generative model:

$$\begin{aligned} X_i &= X_0 + W_i, \quad \forall i = 1, \dots, N \quad \text{where} \\ \text{vec}(X_0) &\sim \mathcal{L}(0, A \otimes C) \quad \text{and} \quad \text{vec}(W_i) \sim \mathcal{L}(0, I_m \otimes B), \end{aligned} \quad (16)$$

where $X_0, W_i \in \mathbb{R}^{n \times m}$ are independent subgaussian random matrices such that $\text{vec}\{X_0\}, \text{vec}\{W_i\} \in \mathbb{R}^{mn}$ have covariances $A \otimes C$ and $I_m \otimes B$, respectively, where recall $\text{vec}\{X_0\}$ and $\text{vec}\{W_i\}$ are obtained by stacking the columns of X_0 and W_i into vectors in \mathbb{R}^{mn} . Here the mean response matrix X_0 and the experiment-specific variation matrices W_i can jointly encode the temporal and spatial dependencies. More generally, we can use a subgaussian random matrix to model replicate-to-replicate fluctuations:

$$\text{vec}\{W_i\} \sim \mathcal{L}(0, I_m \otimes B(t)), \quad \text{where } B(t) \succ 0$$

is the covariance matrix describing the spatial dependencies which may vary cross the N replicated experiments. In this subsection, we consider the general model (16), but with

$$\text{vec}(X_0) \sim \mathcal{N}(0, A \otimes I_n) \quad \text{and} \quad \text{vec}(W_i) \sim \mathcal{N}(0, I_m \otimes B), \quad (17)$$

where X_0 and W_i are independent each other. Note that in model (17), one can avoid the assumption that the trace of A is known. To estimate $\Omega = B^{-1}$, we note that

$$\forall i \neq j, \quad \text{vec}(X_i - X_j) \sim \mathcal{N}(0, I_m \otimes 2B).$$

Without loss of generality, assume N is an even number. We have $N/2$ replicates to estimate $\Omega = B^{-1}$: each column of $\widetilde{W}_i = X_{2i-1} - X_{2i}$ for $i = 1, \dots, N/2$ is a random sample of $\mathcal{N}(0_n, 2B)$. To estimate $\Theta = A^{-1}$, consider the following observed mean response:

$$\bar{X} = \frac{1}{N} \sum_{i=1}^N X_i, \quad \text{where} \quad \text{Cov}(\text{vec}\{\bar{X}\}) = A \otimes I_n + \frac{1}{N} I_m \otimes B. \quad (18)$$

We omit theoretical properties of these estimators. We summarize the estimation procedures as follows:

Algorithm 2-1: Obtain $\hat{\Omega}$ with i.i.d. input vectors $\{\widetilde{W}_i\}_{i=1, \dots, N/2}$

- (1) Let $\tilde{B} := \sum_{i=1}^{N/2} \widetilde{W}_i \widetilde{W}_i^T / (Nm) \succeq 0$ be an unbiased estimator of B .
- (2) Apply graphical Lasso (Friedman et al., 2008) with the input $\tilde{B} \succeq 0$ to obtain $\hat{\Omega}$.

Algorithm 2-2: Obtain $\hat{\Theta}$ with input $\hat{\tau}_B = \text{tr}(\tilde{B})/n$.

Let \tilde{A} be an unbiased estimator of A ; Estimate Θ using Algorithm 1 with

$$\hat{\Gamma} = \tilde{A} := \bar{X}^T \bar{X} / n - \frac{\hat{\tau}_B}{N} I_m, \quad \hat{\Gamma}^{(j)} = \hat{\Gamma}_{-j, -j} \quad \text{and} \quad \hat{\gamma}^{(j)} = \frac{1}{n} \bar{X}_{-j}^T \bar{X}_j.$$

4. Simulation results

We perform simulations to investigate the performances of the estimators. Consider the following covariance models for A and B and their inverses as used in Zhou (2014).

1. AR(1) model : For $\rho \in (0, 1)$, the covariance matrix A is of the form $A = (a_{ij})$ such that $a_{ij} = \rho^{|i-j|}$.
2. Star-Block model: The covariance matrix A consists of sub-blocks with size 16 whose inverses correspond to star graphs, where $A_{ii} = 1$: In each subgraph, five nodes are connected to a central hub node with no other connections. Covariance matrix for each block S in A is generated as follows: $S_{ij} = 0.5$ if $(i, j) \in E$ and $S_{ij} = 0.25$, otherwise.
3. Random graph: The graph is generated according to a Erdos-Renyi random graph model. Initially, we set $\Omega = I_{n \times n}$. Then we randomly select n edges and update Ω as follows: for each new edge (i, j) , a weight $w > 0$ is chosen uniformly at random from $[0.1, 0.3]$; we subtract w from ω_{ij} and ω_{ji} , and increase ω_{ii} and ω_{jj} by w . We multiply the constant $c > 0$ to the

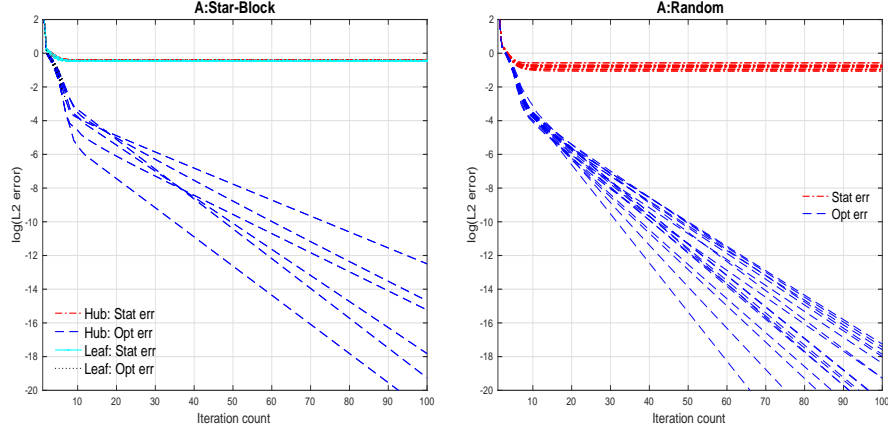


FIGURE 1. Figures display the average of the optimization error $\log(\|\tilde{\beta}_t^i - \hat{\beta}^i\|_2)$ and statistical error $\log(\|\tilde{\beta}_t^i - \beta^i\|_2)$ for $i = 1, \dots, m$ over ten different initial inputs, where $\tilde{\beta}_t^i$ is the t^{th} iterate of the composite gradient descent algorithm on the i^{th} node regression. Each line corresponds to one nodewise regression.

Ω such that $\text{tr}(c^{-1}\Omega^{-1}) = n$ holds, and set $B := c^{-1}\Omega^{-1}$. This sets the trace of B to be n .

Throughout the simulation, we use $\lambda^{(i)} = 2\psi_0\sqrt{\log m/n}$, $b_1 = \sqrt{d_{\max}}$ and step size parameter $\eta = 1.5\lambda_{\max}(A)$ for the composite gradient descent algorithm (8).

4.1. Statistical and optimization error

In this subsection, we study the optimization error $\log(\|\tilde{\beta}_t^i - \hat{\beta}^i\|_2)$ and the statistical error $\log(\|\tilde{\beta}_t^i - \beta^i\|_2)$, based on nodewise regression estimator $\tilde{\beta}_t^i$, which is the t^{th} iteration in the composite gradient descent algorithm for the i^{th} nodewise regression.

Figure 1 displays the error when $m = 512$ and $n = 256$. The matrix A is generated using the Star-Block model (left), and the Erdos-Renyi random graph model with $\|A\|_2 = 3.0$ and $\kappa(A) = 9.0$ (right) respectively, while setting $B = 0.3B^*$, where B^* is generated using the Erdos-Renyi random graph model, where $\|B\|_2 = 0.54$ and $\kappa(B) = 8.40$. For the Star-Block model, we randomly select twenty hubs and twenty leaves linked to hubs are considered in the graph. For the random graph model, we randomly select twenty nodes in the graph.

For each chosen node, the error is averaged over ten trials with different ini-

tialization points in the algorithm. We observe that the sequence of iterates $\{\tilde{\beta}_t^i\}$ to converge geometrically to a fixed point for each node i , while the statistical error flattens out.

4.2. Analysis on statistical error

In the rest of the simulations, we repeat experiments 100 times and record the average of the relative error for estimating Θ using $\hat{\Theta}$ in the operator and the Frobenius norm: $\|\hat{\Theta} - \Theta\|_2 / \|\Theta\|_2$ and $\|\hat{\Theta} - \Theta\|_F / \|\Theta\|_F$. Figure 2 displays the error against a rescaled sample size when $m \in \{128, 256, 512\}$ for each case.

For the top two plots of Figure 2, we consider model (17) when the number of replicates are $N \in \{1, 2, 4, 8\}$. Note that when $N = 1$, the model reduces to the Kronecker sum model. The covariance matrices A and B are generated using the $AR(1)$ and the random model respectively, with $\rho_A = 0.3$ and $\tau_B = 0.5$. We observe the error $\|\hat{\Theta} - \Theta\|$ in the operator and the Frobenius norm decreases as N increases because N reduces the trace effect of B from τ_B to τ_B/N as shown in (18).

For the lower two figures of Figure 2, we consider the Kronecker sum model, where A and B are generated using the Star-Block and $AR(1)$ model, respectively, with $\rho_B \in \{0.3, 0.7\}$ and $\tau_B \in \{0.3, 0.7\}$. We observe that the two sets of curves corresponding to $\tau_B = 0.3$ are lower than those of $\tau_B = 0.7$ while the curves with the lower ρ_B have smaller errors given the same τ_B value. The hidden factor imposed on the upper bound of the relative error $\|\hat{\Theta} - \Theta\|_2 / \|\Theta\|_2$ in the operator norm as stated in Theorem 1 remains invariant for three values of $m \in \{128, 256, 512\}$ when ρ_B and τ_B are fixed. See Remark 1 for discussions.

We observe that the two sets of curves corresponding to $\tau_B = 0.3$ are lower than those of $\tau_B = 0.7$, which can be explained by the fact that the factor has a smaller value when $\tau_B = 0.3$. These results are consistent with the theoretical bounds in Theorem 1. Overall, we see the curves now align for different values of m in the rescaled plots, which confirms the error bound of $O(d\sqrt{\log m/n})$.

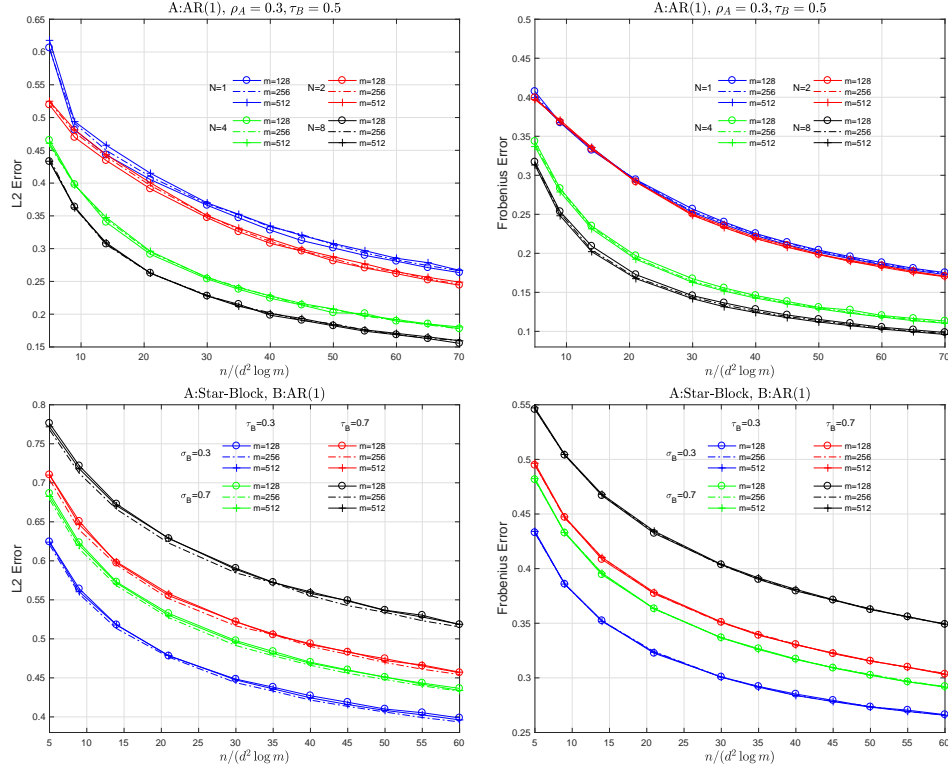


FIGURE 2. The top two plots display the relative L2 (left) and Frobenius (right) errors for the estimates when A follows AR(1) and B follows random model. The bottom two plots display the relative L2 (left) and Frobenius (right) errors when A follows Star-Block and B follows AR(1).

Now we investigate the robustness of the graphical structure in estimated $\hat{\Theta}$ to the specification of $\hat{\tau}_A$. Let E and \hat{E} denote support sets in Θ and $\hat{\Theta}$, respectively, i.e.,

$$E = \{(i, j) : i \neq j, \Theta_{ij} \neq 0\}, \quad \hat{E} = \{(i, j) : i \neq j, \hat{\Theta}_{ij} \neq 0\}.$$

We consider the precision and recall of the estimated \hat{E} :

$$\text{precision} = \frac{|\hat{E} \cap E|}{|\hat{E}|}, \quad \text{recall} = \frac{|\hat{E} \cap E|}{|E|}.$$

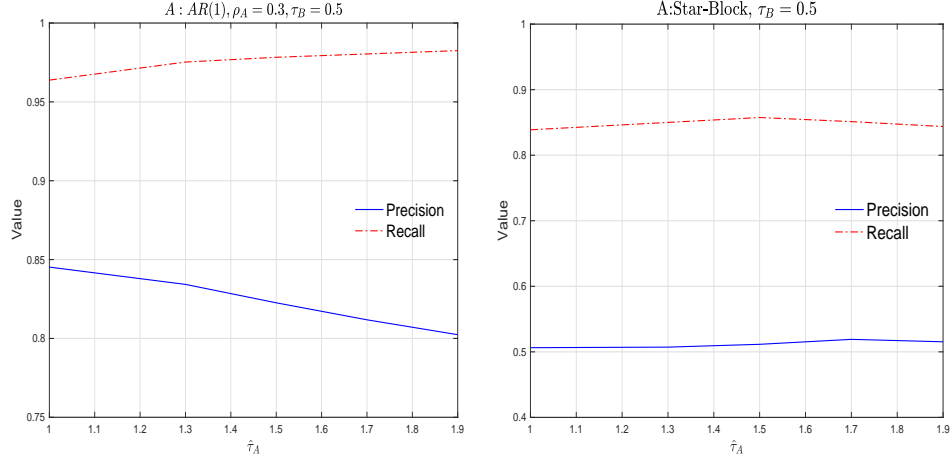


FIGURE 3. The two plots display the precision and recall for the estimated $\hat{\Theta}$ with different specifications of $\hat{\tau}_A$ when $m = 512$, $n = 256$, $\tau_A = 1.5$, and $\tau_B = 0.5$. The left plot is when A follows $AR(1)$ and B follows random model. The right plot is when A follows Star-Block and B follows $AR(1)$.

Figure 3 displays the precision and recall against different specifications of $\hat{\tau}_A \in (1, 1.9)$ when $\tau_A = 1.5$ and $\tau_B = 0.5$. We repeat experiments 100 times and record the average values of the precision and recall for each $\hat{\tau}_A$ case using $\lambda^{(i)} = 2\psi_0\sqrt{\log m/n}$, $b_1 = \sqrt{d}a_{\max}$, and $\eta = 1.5\lambda_{\max}(A)$ in Algorithm 1. For the left plot, A and B are generated using $AR(1)$ and random model, and for the right plot, A and B are generated using Star-Block and $AR(1)$ model, respectively. In the left plot, we observe that $\hat{\tau}_A$ values in $(1, 1.9)$ yield the precisions between 0.8 and 0.85 and recalls between 0.95 and 0.98. In the right plot, the precisions are between 0.50 and 0.52 and recalls are between 0.83 and 0.86. These examples show that the estimated graphical structures have similar performances in terms of precision and recall even when misspecified $\hat{\tau}_A$ values are used.

4.3. Analysis on R-squared

In this subsection, we compare the regular (with no measurement error) and the EIV regression estimators based on R-squared (R^2) values when the true model contains errors in the covariates. Recall the following regular and EIV

regression functions:

$$y = X\beta_1 + \epsilon, \quad \text{where } X \text{ and } y \text{ are observable,} \quad (19)$$

$$y = X_0\beta_2 + \epsilon, \quad X = X_0 + W, \quad \text{where } X \text{ and } y \text{ are observable.} \quad (20)$$

For the regular regression, we consider two regularization methods, ridge regression and Lasso, to estimate β_1 . Lasso provides a sparse solution under the setting that there are no measurement errors. Ridge regression adjusts the gram matrix $X^T X$ by adding some positive constant to all diagonal components, which plays an opposite role compared to the corrected form of gram matrix for the proposed EIV regression. More specifically, Lasso $\hat{\beta}_L$ solves

$$\min_{\beta} \frac{1}{2n} \|y - X\beta\|_2^2 + \lambda_L \|\beta\|_1$$

for some regularization parameter $\lambda_L > 0$. Ridge regression $\hat{\beta}_R$ solves for some regularization parameter $\lambda_R > 0$,

$$\min_{\beta} \frac{1}{n} \|y - X\beta\|_2^2 + \frac{\lambda_R}{n} \|\beta\|_2^2$$

and has a closed form $\hat{\beta}_R = (X^T X + \lambda_R I_p)^{-1} X^T y$. To estimate β_2 for the EIV regression, we apply the composite gradient descent algorithm as in (8).

We compare correlations between fitted and observed values as a R-squared metric to decide on a correct model between the EIV and the regular regression model: calculate the explanatory power of X for y using $R_X^2 = \text{corr}(X\hat{\beta}_1, y)^2$, where $\hat{\beta}_1$ is either the Lasso or ridge regression estimator. Similarly, define the explanatory power of X_0 for y using the EIV estimator $\hat{\beta}_2$:

$$R_{X_0}^2 = \text{corr}(X_0\hat{\beta}_2, y)^2 = \frac{\text{Cov}(y, X_0\hat{\beta}_2)^2}{\text{Var}(y) \text{Var}(X_0\hat{\beta}_2)}. \quad (21)$$

We show in Lemma 5 of the Supplementary materials that when m is fixed, the proposed R^2 metric asymptotically chooses a correct model between the EIV and the regular regression model.

In practice, $R_{X_0}^2$ defined in (50) should be estimated since X_0 is not observed. Under the setting in Theorem 1, we obtain a lower bound of $R_{X_0}^2$ by the function of $\hat{\beta}$, \hat{A}_+ , and \hat{B}_+ , where $\hat{A}_+ := \hat{\Theta}_+^{-1}$ and $\hat{B}_+ := \hat{\Omega}_+^{-1}$. Here $\hat{\Theta}_+$ and $\hat{\Omega}_+$ are the positive definite estimators obtained from Algorithm 3, as summarized in

Section A. Then, we have with high probability

$$R_{X_0}^2 \geq R^* := \frac{\left\{ |\hat{\beta}_2^T X^T y| - \sqrt{2n} \sqrt{1 + \frac{m \log n}{4n}} \|\hat{\beta}_2\|_2 \|y\|_2 \|\hat{B}_+\|_2^{1/2} \right\} \vee 0}{2\|y\|_2^2 \left(n + \frac{m \log n}{4} \right) \|\hat{A}_+\|_2 \|\hat{\beta}_2\|_2^2}. \quad (22)$$

This lower bound R^* will be used instead of the unknown $R_{X_0}^2$. See Section C of the Supplementary materials for detailed mathematical derivations of (22). We compare R^* and R_X^2 to make a correct choice between the EIV and the regular regression model. We consider the following two examples.

Example 1. Let A^* and B^* follow $AR(1)$ model with $\rho_A = 0.5$ and $\rho_B = 0.5$. Consider the EIV regression

$$\begin{aligned} y &= X_0 \beta_2 + \epsilon, \quad X = X_0 + W, \quad \text{where } X \text{ and } y \text{ are observable} \\ \beta_2 &= 0.5 \cdot [1.3, 1.3, 1.1, -1.1, 1, 1, 1, 0.9, 0.9, 1, 0, \dots, 0]^T, \quad \epsilon_i \sim N(0, 1) \end{aligned}$$

with $n = 500$ and $m = 1000$, and $A = \tau_A A^*$ and $B = \tau_B B^*$, where $(\tau_A, \tau_B) = (1.5, 0.5)$.

Example 2. Consider the regular regression

$$\begin{aligned} y &= X \beta_1 + \epsilon, \quad \text{where } X \text{ and } y \text{ are observable,} \\ \beta_1 &= 0.5 \cdot [1.3, 1.3, 1.1, -1.1, 1, 1, 1, 0.9, 0.9, 1, 0, \dots, 0]^T, \quad \epsilon_i \sim N(0, 1) \end{aligned}$$

with $n = 500$ and $m = 1000$, and the rows of X are i.i.d. $N(0, A)$, where the covariance matrix is $A = 2A^*$ and A^* follows $AR(1)$ model with $\rho_A = 0.5$.

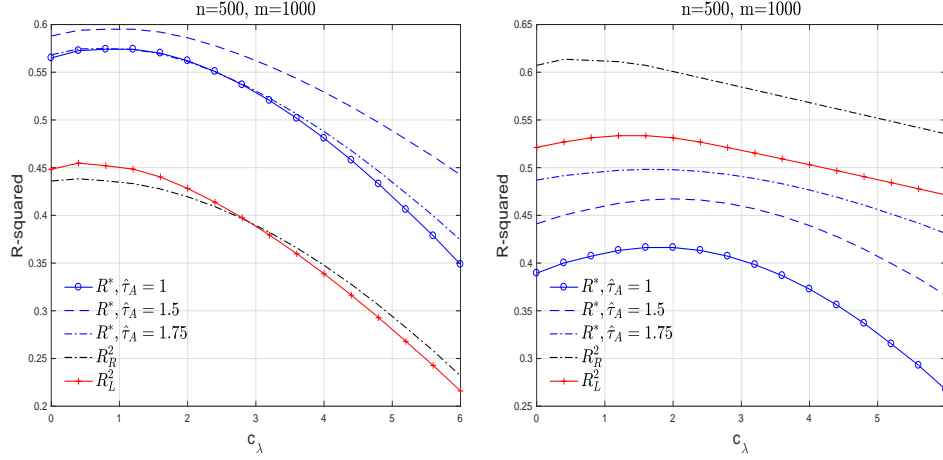


FIGURE 4. The first plot shows the lower bound of the R-squared values of EIV regression (i.e., R^*), and the calculated R-squared values for the Lasso (R_L^2) and ridge regression (R_R^2) when the actual model follows the EIV model with $(\tau_A, \tau_B) = (1.5, 0.5)$ (Example 1). The second plot considers the case in which the actual model follows regular linear model (Example 2).

We apply the EIV and regular regressions, that is, Lasso and ridge regression without measurement errors, to models in Examples 1-2. For the Lasso and EIV, the regularization parameters $\{c_\lambda \sqrt{\log m/n} \mid c_\lambda \in (0, 6)\}$ are used. For the ridge regression, the regularization parameters $\{nc_\lambda \mid c_\lambda \in (0, 6)\}$ are used. The first plot of Figure 4 shows R_X^2 and R^* values averaged over 100 trials when the true model follows EIV (Example 1). We observe that R^* is generally larger than R-squared values of Lasso (R_L^2) and ridge regression (R_R^2) even when misspecified $\hat{\tau}_A$ values are used. The second plot of Figure 4 shows R^2 values when the true model does not involve errors-in-variables (Example 2). We see that R_L^2 and R_R^2 are larger than R^* obtained by the EIV regression.

These findings show that comparison based on R^2 values of the EIV regression versus the Lasso or Ridge regression can help distinguish one regression model from the other and the EIV regression model is robust to the specification of τ_A .

5. Analysis of hawkmoth neural encoding data

In the experiments conducted by Sponberg and Daniel (2012) and Sponberg et al. (2015), the neural firing time was measured using electrical probes, and the torque was measured via an optical torque meter. For each of the 7 hawkmoths

indexed $i = 1, \dots, 7$, data for n_i wing strokes were obtained. For a single wing stroke, the measured torque $X^{(i)} \in \mathbb{R}^{n_i \times 500}$ consists of 500 sampled torque values spanning the duration of the wing stroke. Let $\Delta^{(i)} \in \mathbb{R}^{n_i}$ be the Δ values for moth i , obtained at the beginning of each wing stroke. Two pre-processing approaches give rise to separate “spike-triggered” and “phase-triggered” data sets. We omit the index i when no confusion arises.

5.1. Generating model

The data $X^{(i)}$ for one moth can be viewed as a matrix-variate observation, with one axis (rows) indexing wing strokes, and the other axis (columns) corresponding to time points within a wing stroke. The Kronecker sum model decomposes this observation into two latent terms. One of these terms has independent rows (wing strokes) and dependent columns (time points), and the other term has dependent rows and independent columns. Our primary question here is whether the information in $X^{(i)}$ that is related to $\Delta^{(i)}$ is concentrated in only one of these two latent terms. This would suggest that the other term may contain motion features that are not strongly neurally encoded, for example measurement noise.

For ease of visualization, in the graphical analysis the rows of the torque data $X^{(i)}$ are sorted in descending order by the corresponding Δ . Figure 10 in the Supplementary materials shows heat maps of the sample correlation matrix of 500 temporal points and the sample correlation matrix of wing strokes, showing dependencies in both time points and among the wing strokes. We will use the Kronecker sum model to explain these two-way dependencies in the torque data, and EIV regression to explore the joint relationship between neural firing and torque.

We decompose the observed torque data X as

$$X_{ij} = R_i + C_j + \phi_{ij} \quad \text{for } i = 1, \dots, n, j = 1, \dots, 500, \quad (23)$$

where R_i and C_j represent the i th row mean and j th column mean of X , respectively (when $\sum_{ij} X_{ij} = 0$). The matrix form of (23) is

$$X = R1^T + 1C^T + \Phi, \quad (24)$$

where 1 is the vector of ones, $\Phi_{n \times 500} = (\phi_{ij})$, $R = (R_1, \dots, R_n)^T$ and $C = (C_1, \dots, C_{500})^T$. In Table 1, we show the composition of three components in

(24) through $\|R1^T\|_F^2/\|X\|_F^2$, $\|1C^T\|_F^2/\|X\|_F^2$ and $\|\Phi\|_F^2/\|X\|_F^2$. We see that column effects are negligible and at least 70% of the variation in the data can be explained by Φ for all moths. As noted above, the row means are already known to be a major determinant of the spike times Δ . Therefore, all analysis is based on the row-centered data $\tilde{X} = X - R1^T$, to focus on the possible existence of additional neurally-encoded features in the wing strokes.

TABLE 1
Proportion of each part in data.

Proportion	J	K	L	M	N	P	Q
$\ R1^T\ _F^2/\ X\ _F^2$	0.08	0.09	0.27	0.11	0.22	0.06	0.18
$\ 1C^T\ _F^2/\ X\ _F^2$	0.02	0.01	0.01	0.02	0.01	0.02	0.01
$\ \theta\ _F^2/\ X\ _F^2$	0.71	0.90	0.71	0.87	0.76	0.91	0.80

5.2. Interpretation of the graphical structure

In this subsection, we discuss the graphical structures of the fitted covariance matrices A and B from the Kronecker sum model. Without loss of generality we scale \tilde{X} so that its overall variance is 2.

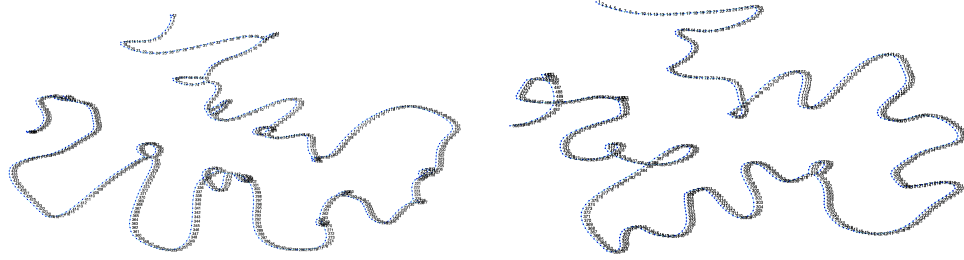


FIGURE 5. The graphical structure of $\hat{\Theta}$ when $\hat{\tau}_A = 1.5$ and $\lambda_A^{(i)} = 0.5\sqrt{\frac{\log 500}{n}} \asymp 0.05$ for moth J (left) and L (right). Edges (i, j) with $|\hat{\Theta}_{ij}| > 0.05$ are connected in the graph.

Figure 5 displays the graphical structures of the estimator $\hat{\Theta}$ for the Kronecker sum model when $\hat{\tau}_A = 1.5$. It is apparent that both graphs have a chain structure, with some loops, which is expected because $\hat{\Theta}$ encodes the conditional dependency relationships between and across time points, and the observed torque data (across time points) are therefore strongly autocorrelated.

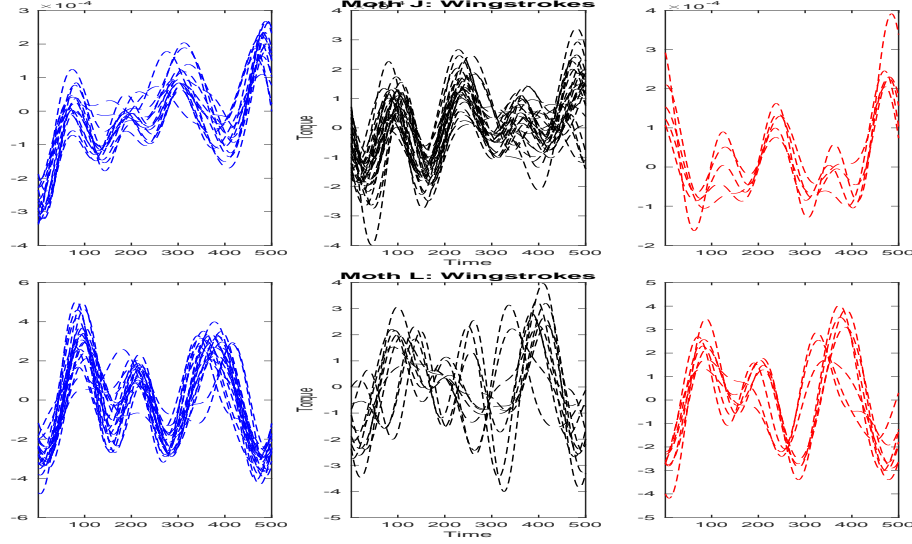


FIGURE 6. Torque ensembles for selected three clusters for moth J (top) and L (bottom).

We select the three largest clusters of wing strokes from the estimated structure of Ω when $\hat{\tau}_A = 1.5$. See Figures 8-9 of the Supplementary materials for graphical structure of $\hat{\Omega}$. Figure 6 displays torque ensembles of the three clusters for moth J and L, respectively. It is seen that the wing strokes from the same cluster are highly correlated or highly anti-correlated, which implies that the structural information encoded in $\hat{\Omega}$ is not arbitrary and indeed captures strong dependencies among wing strokes.

5.3. Regression analysis of torque and DLM

In this subsection, we analyze the relationship between the neural firing time and torque ensemble data utilizing various regression methods, including EIV regression. In the EIV regression, we model $\text{Cov}(\text{vec} \left\{ \tilde{\mathbf{X}} \right\})$ using the Kronecker sum structure, as elaborated in the previous section.

We first perform simple linear regression of $\Delta = t_L - t_R$ on the mean torque (μ) to regress out the mean torque effect from Δ . Denote by $\tilde{\Delta}$ the residual vector:

$$\tilde{\Delta} := \Delta - \alpha - \beta\mu, \quad \alpha = \bar{\Delta} - \beta\bar{\mu}, \quad \beta = \frac{\text{Cov}(\mu, \Delta)}{\text{Var}(\mu)}, \quad (25)$$

where $\bar{\Delta}$ and $\bar{\mu}$ are the means of the components in Δ and μ , respectively. We will treat $\tilde{\Delta}$ as a response vector and fit a separate linear model to each hawkmoth,

to explore the possibility that the average torque μ does not capture all the information in Δ .

We then fit both regular regression (26) and EIV regression model (27), as previously studied in Rudelson and Zhou (2017), to relate the residual neural spike time differences (25) and torque values:

$$\tilde{\Delta} = \tilde{X}\beta_1 + \epsilon, \quad \text{where } \tilde{X} \text{ and } \tilde{\Delta} \text{ are observable;} \quad (26)$$

$$\tilde{\Delta} = X_0\beta_2 + \epsilon, \quad \tilde{X} = X_0 + W, \quad \text{where } \tilde{X} \text{ and } \tilde{\Delta} \text{ are observable.} \quad (27)$$

By using the R-squared analysis from the above EIV regression, we will argue that variation in $\tilde{\Delta}$ is more strongly related to the latent X_0 in model (27) compared to the observed \tilde{X} .

Based on the fact that $\beta_1, \beta_2 \in \mathbb{R}^{500}$ are coefficient vectors whose domain is a temporal space, we aim to obtain smoothed estimators for β_1 and β_2 to explain the variation in $\tilde{\Delta}$. Toward this goal, we use B-spline basis functions to approximate these coefficients. Let $\pi_1(t), \dots, \pi_{k_n+l}(t)$ be the normalized B-spline basis functions of order l with k_n quasi-uniform knots. We set $l = 3$ and $k_n = 17$, so we use $K_n := k_n + l = 20$ basis functions. Let $\tilde{\Pi}_{t,k} = \pi_k(t)$ for $t = 1, 2, \dots, 500$ and $k = 1, 2, \dots, K_n$. We use an orthonormal basis for the column space of $\tilde{\Pi}$ obtained through QR decomposition, denoted by $\Pi \in \mathbb{R}^{500 \times K_n}$, that is, $\Pi^T \Pi = I_{K_n}$. Upon estimating ζ_k , we obtain estimators of the β_k via the relationship $\beta_k = \Pi \zeta_k$, where $\zeta_k \in \mathbb{R}^{K_n \times 1}$. Note that this relationship preserves at least 95% of the variance of the data \tilde{X} in the sense that $\|\tilde{X}\Pi\|_F^2 \geq 0.95\|\tilde{X}\|_F^2$ for all moths.

Models (26) and (27) can now be rewritten as

$$\tilde{\Delta} = \tilde{X}\Pi\zeta_1 + \epsilon, \quad \text{where } \tilde{X}\Pi \text{ and } \tilde{\Delta} \text{ are observable;} \quad (28)$$

$$\tilde{\Delta} = X_0\Pi\zeta_2 + \epsilon, \quad \tilde{X}\Pi = X_0\Pi + W\Pi, \quad (29)$$

where $\tilde{X}\Pi$ and $\tilde{\Delta}$ are observable.

Note that the model (55) still follows the EIV model as in Rudelson and Zhou (2017), since the covariance matrix of $\text{vec}\{\tilde{X}\Pi\}$ is

$$\text{Cov}(\text{vec}\{\tilde{X}\Pi\}) = \Gamma_A \oplus B, \quad \text{where } \Gamma_A := \Pi^T A \Pi.$$

See Subsection H.2 of the Supplementary materials for details.

We obtain $\hat{\zeta}_1$, an estimator of ζ_1 using ridge regression or the Lasso by treating $\tilde{X}\Pi$ as a design matrix. We obtain the estimator $\hat{\zeta}_2$ of ζ_2 by solving EIV

regression (5) with $\hat{\tau}_B = \left(\frac{1}{500n} \|\tilde{X}\|_F^2 - \tau_A \right)_+$ and

$$\hat{\Gamma} = \frac{1}{n}(\tilde{X}\Pi)^T \tilde{X}\Pi - \hat{\tau}_B I \quad \text{and} \quad \hat{\gamma} = \frac{1}{n}(\tilde{X}\Pi)^T \tilde{\Delta},$$

where $\hat{\Gamma}$ is an unbiased estimator of Γ_A . For the objective function (5), we choose $b_1 = 2\|\hat{\zeta}_1\|_1$ and step size parameter $\eta = 0.5\|\hat{\Gamma}\|_2$ for the composite gradient descent algorithm, where $\hat{\zeta}_1$ is the Lasso estimator. Then we obtain estimators $\hat{\beta}_1 = \Pi\hat{\zeta}_1$ and $\hat{\beta}_2 = \Pi\hat{\zeta}_2$.

We calculate the explanatory power of \tilde{X} for $\tilde{\Delta}$ using the proportion of explained variance as follows: $R_{\tilde{X}}^2 = \text{corr}(\tilde{X}\hat{\beta}_1, \tilde{\Delta})^2$. We record the lower bound of the explanatory power of X_0 for $\tilde{\Delta}$ using the estimator $\hat{\beta}_2$:

$$R_{X_0}^2 = \text{corr}(X_0\hat{\beta}_2, \tilde{\Delta})^2 \geq R^*, \quad (30)$$

where R^* is defined in (22).

Table 2 shows the values of $R_{\tilde{X}}^2$ obtained for ridge regression and the Lasso, denoted respectively as $R_{\tilde{X}}^2(Ridge)$ and $R_{\tilde{X}}^2(Lasso)$. We record the maximum value of $R_{\tilde{X}}^2(Lasso)$ and R^* among the values obtained from the solution paths with the regularization parameters $c_\lambda \sqrt{\log K_n/n}$, where $c_\lambda \in (0, 7)$. To obtain R^* , we consider the EIV with $\hat{\tau}_A \in \{0.1, 0.2, \dots, 1.9\}$. Similarly, we record the maximum value of $R_{\tilde{X}}^2(Ridge)$ among the values obtained from the ridge regression solution path with the regularization parameters nc_λ , where $c_\lambda \in (0, 7)$. While the Kronecker sum model is not sufficient to identify τ_A from the random matrix X alone, when considered in the context of a regression analysis we can identify τ_A by maximizing the R^2 values of the regression between the responses and the latent component X_0 . We record the optimal $\hat{\tau}_A$ that provides the highest R^* value.

TABLE 2
Explanatory power (R^2)

Spike	$R_{\tilde{X}}^2(Ridge)$	$R_{\tilde{X}}^2(Lasso)$	$\hat{\tau}_A$	EIV $R_{X_0}^2(R^*)$
J	0.12	0.12	1.4	0.20
K	0.12	0.11	1.4	0.22
L	0.15	0.18	1.4	0.26
M	0.02	0.02	1.5	0.17
N	0.15	0.21	1.3	0.28
P	0.19	0.19	1.5	0.29
Q	0.19	0.21	1.4	0.35

In all cases, R^* , the lower bound of $R_{X_0}^2$ obtained from errors-in-variables regression, is greater than $R_{\tilde{X}}^2$ obtained from the Lasso and Ridge regression. This suggests that the torque signal component X_0 expressed in the Kronecker sum model may be viewed as a denoised torque signal, and that this denoised torque signal is more strongly correlated to the motor signal than the observed torque signal.

To ensure that this increase in R^2 values as summarized in Table 2 is not due to chance or overfitting, we randomly permute the components of Δ and refit the regression models, while keeping \tilde{X} intact. We summarize the R^* values in Table 3, and observe that all the obtained R^* values are between zero and 0.05. Combined with the simulation results presented in Figure 4 in Subsection 4.3, this implies that the increase in R^2 values reflects a true relationship between $\tilde{\Delta}$ and the latent component of \tilde{X} , and is not due to chance or overfitting.

TABLE 3
Explanatory power (R -squared)

Spike	$R_{\tilde{X}}^2(Ridge)$	$R_{\tilde{X}}^2(Lasso)$	$R_{X_0}^2(R^*)$
J	0.01	0.01	0.01
K	0.02	0.03	0.02
L	0.02	0.01	0.02
M	0.01	0.02	0.01
N	0.03	0.03	0.04
P	0.01	0.01	0.00
Q	0.00	0.01	0.00

6. Conclusion

Data with complex dependencies arise in many settings, for example when a large number of replicated experiments are run on subjects in a research study, a practice that is common in psychology, linguistics, neuroscience, and other areas. The Kronecker sum provides a non-separable alternative to widely-used separable covariance models such as the Kronecker product, and may fit data better in some circumstances.

We illustrate these new methods and theory using data from a neural encoding study of hawkmoth flight behavior. We provide two novel insights about these data. First, we illustrate that although the mean torque (per wing stroke) captures a substantial fraction of the neurally encoded flight turning behavior,

additional components of the wing stroke trajectory also appear to be neurally encoded. Second, we show that the observed flight torque trajectories can be decomposed into two latent components, with one component capturing the majority of the neurally encoded behavior. The latter observation provides a promising basis for characterizing neural encoding using latent structures.

TABLE 4
The Symbols

Parameters	Definitions
X_i	The i th column of a matrix X
X_{-i}	The sub-matrix of X without the i th column
$X_{-i,-j}$	The sub-matrix of X without the i th row and j th column
τ_Σ	$\text{tr}(\Sigma)/p$ for a square matrix $\Sigma \in \mathbb{R}^{p \times p}$
Θ	A^{-1}
Ω	B^{-1}
a_{\max}	$\max_i A_{ii}$
b_{\max}	$\max_i B_{ii}$
α	$\frac{5}{8} \lambda_{\min}(A)$
$\eta \geq \frac{11}{8} \lambda_{\max}(A)$	step size parameter
$\varphi(s_0)$	$\rho_{\max}(s_0, A) + \tau_B$
τ_0	$\frac{400C^2 \varphi(s_0+1)^2}{\lambda_{\min}(A)}$
D'_0	$\ B\ _2^{1/2} + a_{\max}^{1/2}$
\tilde{D}'_0	$\ A\ _2^{1/2} + b_{\max}^{1/2}$
D_{oracle}	$2(\ A\ _2^{1/2} + \ B\ _2^{1/2})$
$\tau_B^{+/2}$	$\sqrt{\tau_B} + \frac{D_{\text{oracle}}}{\sqrt{m}}$
K	$\sup_{p \geq 1} p^{-1/2} (\mathbb{E} X ^p)^{1/p}$ for $X \sim N(0, 1)$
C_ψ	$K^2 C_0 D'_0 \left(\tau_B^{+/2} \kappa(A) + \sqrt{a_{\max}} \right)$
ψ_0	$0.1 D'_0 \left(\tau_B^{+/2} a_{\max} + \sqrt{a_{\max}} \right)$
$\rho_{\max}(d, A)$	$\max_{t \neq 0; d\text{-sparse}} \ At\ _2^2 / \ t\ _2^2$
$\varphi(s_0)$	$\rho_{\max}(s_0, A) + \tau_B$
s_0	The largest integer satisfying $\sqrt{s_0} \varphi(s_0) \leq \frac{\lambda_{\min}(A)}{32C} \sqrt{\frac{n}{\log m}}$
ψ_1^2	$\frac{16c}{\lambda_{\min}(A)} \left(\frac{1}{1-\kappa} + \frac{\lambda_{\min}(A)}{2s_0} \right)$

Supplementary materials

This supplementary material is organized as follows. Section A introduces an additional estimation procedure of Θ as described in Section 2 of the main paper. Section B includes details of theoretical properties of the estimator, and main lemmas are presented in Section C. Proofs of Theorem 1 is included in Section D. Section E shows the consistency of the estimator $\hat{\Omega}$. Section F contains the proofs of lemmas. Section G shows details of R-squared analysis. Section H includes additional real data analysis. Section I includes additional tables and figures.

Theorem 3 is directly from Rudelson and Zhou (2017) by adopting the node-wise regression case with Gaussian random ensembles. Theorems 1 and 4 show estimation error bound for $\hat{\Theta}$ and $\hat{\Omega}$. We emphasize that Lemma 1 holds for a subgaussian model while Lemma 2 assumes Gaussian model. We note that Lemma 4 is included in Rudelson and Zhou (2017) and Lemma 3 is directly from the existing Lemma in Rudelson and Zhou (2017) by applying to the nodewise regression setting (i.e., Gaussian model). Lemma 5 shows the asymptotic property of R-squared metric based on Gaussian model. Lemma 6 is used to obtain the lower bound of R-squared values for errors-in-variables regression estimate in high-dimensional settings based on subgaussian model.

Appendix A: Additional estimation procedure

The estimated $\hat{\Theta}$ and $\hat{\Phi}$ obtained from Algorithm 1 in the main paper are not necessarily positive-semidefinite. To obtain positive-semidefinite estimated precision matrices, one can consider the following additional estimation procedure.

Algorithm 3: Obtain $\hat{\Theta}_+$ with an input $\hat{\Theta}$

Consider the case in which $\hat{\Theta}$ is not positive-semidefinite. Since $\hat{\Theta}$ is symmetric, there exists an orthogonal matrix U and a diagonal matrix $D = \text{diag}(\lambda_1, \dots, \lambda_m)$ such that $\hat{\Theta} = UDU^T$, where $\lambda_1 \leq \dots \leq \lambda_m$. Since $\hat{\Theta}$ is not positive-semidefinite, $\lambda_1 < 0$. Let $\hat{\Theta}_+ = UD_+U^T$, where $D_+ := \text{diag}(\lambda_1 \vee \epsilon, \dots, \lambda_m \vee \epsilon)$ for some positive constant $0 < \epsilon \leq -\lambda_1$. Then $\hat{\Theta}_+$ is positive-semidefinite and satisfies with high probability

$$\|\hat{\Theta}_+ - \Theta\|_2 \leq \|\hat{\Theta} - \hat{\Theta}_+\|_2 + \|\hat{\Theta} - \Theta\|_2 \leq -2\lambda_1 + \|\hat{\Theta} - \Theta\|_2 \leq 3\|\hat{\Theta} - \Theta\|_2.$$

The estimator $\hat{\Theta}_+$ is positive-semidefinite and has error bound at the same order with $\hat{\Theta}$ as in Theorem 1. In practice, we set $\epsilon = -\lambda_1$.

Appendix B: Theoretical property

B.1. Assumption

In this subsection, we define some notations and assumptions which facilitate the theoretical properties of the proposed estimator. We will define some parameters related to the restricted and sparse eigenvalue conditions. We first state Definitions 1-2. For more details of these, see Rudelson and Zhou (2017).

Definition 1. (Restricted eigenvalue condition $\text{RE}(s_0, k_0, A)$) Let $1 \leq s_0 \leq m$ and k_0 be a positive number. The $m \times m$ matrix A satisfies $\text{RE}(s_0, k_0, A)$ condition with parameter $K(s_0, k_0, A)$ if for any $v \neq 0$,

$$\frac{1}{K(s_0, k_0, A)} := \min_{\substack{J \subseteq \{1, \dots, p\}, \\ |J| \leq s_0}} \min_{\|v_{J^c}\|_1 \leq k_0 \|v_J\|_1} \frac{\|Av\|_2}{\|v_J\|_2} > 0, \quad (31)$$

where v_J represents the subvector of $v \in \mathbb{R}^m$ confined to a subset J of $\{1, \dots, m\}$.

We also consider the following variation of the baseline RE condition.

Definition 2. (Lower-RE condition) (Loh and Wainwright, 2012; Rudelson and Zhou, 2017) The $m \times m$ matrix Γ satisfies a Lower-RE condition with curvature $\alpha > 0$ and tolerance $\tau > 0$ if

$$\theta^T \Gamma \theta \geq \alpha \|\theta\|_2^2 - \tau \|\theta\|_1^2, \quad \forall \theta \in \mathbb{R}^m.$$

Definition 3. (Upper-RE condition) The $m \times m$ matrix Γ satisfies an upper-RE condition with curvature $\bar{\alpha} > 0$ and tolerance $\tau > 0$ if

$$\theta^T \Gamma \theta \leq \bar{\alpha} \|\theta\|_2^2 + \tau \|\theta\|_1^2, \quad \forall \theta \in \mathbb{R}^m.$$

Definition 4. Define the largest and smallest d -sparse eigenvalue of a $m \times m$ matrix A : for $d < m$,

$$\rho_{\max}(d, A) := \max_{t \neq 0; \|t\|_0 \leq d} \frac{\|At\|_2^2}{\|t\|_2^2}, \quad (32)$$

$$\text{and } \rho_{\min}(d, A) := \min_{t \neq 0; \|t\|_0 \leq d} \frac{\|At\|_2^2}{\|t\|_2^2}. \quad (33)$$

Recall that we consider the inverse covariance matrices $\Theta = A^{-1}$ and $\Omega = B^{-1}$ in the additive model of $X = X_0 + W$ such that

$$\text{vec}\{X\} \sim \mathcal{N}(0, \Sigma) \quad \text{where} \quad \Sigma = A \oplus B := A \otimes I_n + I_m \otimes B. \quad (34)$$

We have also stated the subgaussian analog of (34) in (3). Throughout this supplement, we use the Gaussian ensemble design for the main results, while noting that the more general subgaussian random design model as in (3) is allowed in order for some of key concentration of measure bounds to go through.

Let $s_0 \geq 1$ be the largest integer chosen such that the following inequality holds:

$$\sqrt{s_0} \varphi(s_0) \leq \frac{\lambda_{\min}(A)}{32C} \sqrt{\frac{n}{\log m}}, \quad \varphi(s_0) := \rho_{\max}(s_0, A) + \tau_B, \quad (35)$$

where $\tau_B = \text{tr}(B)/n$ and C is to be defined. Denote by

$$M_A = \frac{64C\varphi(s_0)}{\lambda_{\min}(A)} \geq 64C. \quad (36)$$

We use the expression $\tau := (\lambda_{\min}(A) - \alpha)/s_0$, where $\alpha = 5\lambda_{\min}(A)/8$.

B.2. EIV regression

We first review theoretical properties of the EIV regression estimator in the following theorem on the subgaussian model (3), which is directly from Rudelson and Zhou (2017).

Theorem 2. (Estimation for the Lasso-type estimator) [Theorem 3 of Rudelson and Zhou (2017)] Suppose $n = \Omega(\log m)$ and $n \leq (\mathcal{V}/e)m \log m$, where \mathcal{V} is a constant which depends on $\lambda_{\min}(A)$, $\rho_{\max}(s_0, A)$ and $\text{tr}(B)/n$. Suppose m is sufficiently large. Suppose (A1)-(A4) hold. Consider the EIV regression model (1) and 3 as defined in the main paper with independent random matrices X_0, W as in (3) and $\|\epsilon_j\|_{\psi_2} \leq M_\epsilon$. Let $C_0, c' > 0$ be some absolute constants. Let $D_2 := 2(\|A\|_2 + \|B\|_2)$. Suppose that $c'K^4 \leq 1$ and

$$r(B) := \frac{\text{tr}(B)}{\|B\|_2} \geq 16c'K^4 \frac{n}{\log m} \log \frac{\mathcal{V}m \log m}{n}. \quad (37)$$

Let b_0, ϕ be numbers which satisfy

$$\frac{M_\epsilon^2}{K^2 b_0^2} \leq \phi \leq 1. \quad (38)$$

Assume that the sparsity of β^* satisfies for some $0 < \phi \leq 1$

$$d := |\text{supp}(\beta^*)| \leq \frac{c'\phi K^4}{40M_+^2} \frac{n}{\log m} < n/2, \quad (39)$$

$$\text{where } M_+ = \frac{32C\varpi(s_0 + 1)}{\lambda_{\min}(A)} \quad (40)$$

for $\varpi(s_0 + 1) = \rho_{\max}(s_0 + 1, A) + \tau_B$. Let $\hat{\beta}$ be an optimal solution to the EIV regression with

$$\lambda \geq 4\psi \sqrt{\frac{\log m}{n}} \quad \text{where } \psi := C_0 D_2 K (K \|\beta^*\|_2 + M_\epsilon). \quad (41)$$

Then for any d -sparse vectors $\beta^* \in \mathbb{R}^m$, such that $\phi b_0^2 \leq \|\beta^*\|_2^2 \leq b_0^2$, we have with probability at least $1 - 16/m^3$,

$$\|\hat{\beta} - \beta^*\|_2 \leq \frac{20}{\alpha} \lambda \sqrt{d} \quad \text{and} \quad \|\hat{\beta} - \beta^*\|_1 \leq \frac{80}{\alpha} \lambda d.$$

B.3. Multiple EIV regressions for the Gaussian Random Ensembles

First, we define some constants:

$$D_0 = \sqrt{\tau_B} + \sqrt{a_{\max}}, \quad D'_0 = \|B\|_2^{1/2} + \sqrt{a_{\max}}, \quad \tau_B^+ := (\tau_B^{+/2})^2, \quad (42)$$

$$\tau_B^{+/2} := \sqrt{\tau_B} + \frac{D_{\text{oracle}}}{\sqrt{m}}, \quad D_{\text{oracle}} = 2 \left(\sqrt{\|A\|_2} + \sqrt{\|B\|_2} \right). \quad (43)$$

The following theorem 3 shows oracle inequalities of the nodewise regressions, which is analogous to Theorem 6 of Rudelson and Zhou (2017), which is adapted to the Gaussian random ensembles when generating data (34). Theorem 3 will be used for the proof of Theorem 1 as in Section D.

Theorem 3. *Consider the Kronecker sum model as in (34). Suppose all conditions in Theorem 2 hold, except that we drop (38) and replace (41) with*

$$\lambda^{(i)} \geq 4\psi_i \sqrt{\frac{\log m}{n}} \quad \text{where} \quad \psi_i := C_0 D'_0 K^2 \left(\tau_B^{+/2} \|\beta^i\|_2 + \sigma_{V_i} \right), \quad (44)$$

where $\sigma_{V_i}^2 := A_{ii} - A_{i,-i} A_{-i,-i}^{-1} A_{-i,i}$. Suppose that for $0 < \phi \leq 1$ and $C_A := \frac{1}{160M_+^2}$,

$$d := \max_{1 \leq i \leq m} |\text{supp}(\beta^i)| \leq C_A \frac{n}{\log m} \{c' c'' D_\phi \wedge 8\}, \quad \text{where} \quad (45)$$

$$c'' := \frac{\|B\|_2 + a_{\max}}{\varpi(s_0 + 1)^2}, \quad D_\phi = \frac{K^2 M_\epsilon^2}{b_0^2} + K^4 \tau_B^+ \phi,$$

and c', ϕ, b_0 as defined in Theorem 2. We obtain m vectors of $\hat{\beta}^i, i = 1, \dots, m$ by solving (7) in the main paper with $\lambda = \lambda^{(i)}$,

$$\hat{\Gamma}^{(i)} = \frac{1}{n} X_{-i}^T X_{-i} - \hat{\tau}_B I_{m-1} \quad \text{and} \quad \hat{\gamma}^{(i)} = \frac{1}{n} X_{-i}^T X_i,$$

for each i . Let $b_1 := b_0 \sqrt{d}$. Then for all d -sparse vectors $\beta^i \in \mathbb{R}^{m-1}, i = 1, \dots, m$, such that $\phi b_0^2 \leq \|\beta^i\|_2^2 \leq b_0^2$, we have with probability at least $1 - 16/m^2$,

$$\|\hat{\beta}^i - \beta^i\|_2 \leq \frac{20}{\alpha} \lambda^{(i)} \sqrt{d} \quad \text{and} \quad \|\hat{\beta}^i - \beta^i\|_1 \leq \frac{80}{\alpha} \lambda^{(i)} d.$$

Appendix C: Main Lemmas

The following lemmas are essential to prove the main theorems. Lemmas 1 and 2 are analogous to Theorem 26 and Corollary 13 of Rudelson and Zhou (2017), respectively. We emphasize that Lemma 1 holds for a subgaussian model while Lemma 2 assumes Gaussian model.

Lemma 1. Suppose (A1) holds. Let $A_{m \times m}$ and $B_{n \times n}$ be positive definite covariance matrices. Let Z and X be $n \times m$ random matrices as defined in Theorem 2. Let

$$\Delta := \widehat{\Gamma}_A - A := \frac{1}{n} X^T X - \widehat{\tau}_B I_m - A. \quad (46)$$

Let $D_1 := \frac{\|A\|_F}{\sqrt{m}} + \frac{\|B\|_F}{\sqrt{n}}$, $\varphi = \|B\|_2 + a_{\max}$, and $\psi_0 = \varphi C_0 K^2 / \sqrt{c'}$. Then with probability at least $1 - 6/m^2 - 6/m^3$,

$$|\Delta|_{\max} \leq 12CK^2\varphi\sqrt{\frac{\log m}{n}} = O\left(\psi_0\sqrt{\frac{\log m}{n}}\right),$$

where C_0 is appropriately chosen and c' sufficiently small.

Lemma 2. Suppose (A1) holds. Suppose that $m \geq 16$ and $\frac{\|B\|_F^2}{\|B\|_2^2} \geq \log m$. Let $\widehat{\Gamma}^{(i)}$ and $\widehat{\gamma}^{(i)}$ be as defined in Algorithm 1 in the main paper. Let $D_0, D'_0, D_{\text{oracle}}$, and $\tau_B^{+/2}$ be as defined in (42) and (43). On event \mathcal{B}_0 , we have for some absolute constant C_0 , for all i ,

$$\left\| \widehat{\gamma}^{(i)} - \widehat{\Gamma}^{(i)} \beta^i \right\|_{\infty} \leq \psi_i \sqrt{\frac{\log m}{n}}, \quad (47)$$

where

$$\psi_i := C_0 K^2 D'_0 \left(\tau_B^{+/2} \|\beta^i\|_2 + \sigma_{V_i} \right) \leq C_0 K^2 D'_0 (\tau_B^{+/2} \kappa(A) + \sigma_V),$$

where recall $D'_0 = \|B\|_2^{1/2} + a_{\max}^{1/2}$ and $\sigma_V := \max_j \sigma_{V_j}$. Then, $\mathbb{P}(\mathcal{B}_0) \geq 1 - 16/m^2$.

Appendix D: Proof of Theorem 1

Lemmas 1 and 2 show that the following conditions hold with probability at least $1 - 20/m^2 - 6/m^3$:

$$\left\| \widehat{\gamma}^{(i)} - \widehat{\Gamma}^{(i)} \beta^i \right\|_{\infty} \leq C_{\psi} \sqrt{\frac{\log m}{n}},$$

$$\left| \widehat{\Gamma}_A - A \right|_{\max} = \left| \frac{1}{n} X^T X - \widehat{\tau}_B I_m - A \right|_{\max} = O\left(C_{\psi} \sqrt{\frac{\log m}{n}}\right),$$

where $C_{\psi} := K^2 C_0 D'_0 (\tau_B^{+/2} \kappa(A) + \sqrt{a_{\max}})$. Next we see that the lower-RE condition holds with curvature $\alpha = 5\lambda_{\min}(A)/8$ and tolerance $\tau = \frac{\lambda_{\min}(A)}{2s_0}$

uniformly over the matrices $\widehat{\Gamma}^{(i)}$ with scaling as required by Corollary 5 in [Loh and Wainwright \(2012\)](#), namely,

$$\sqrt{d}\tau \leq \min \left\{ \frac{\alpha}{32\sqrt{d}}, \frac{\lambda^{(i)}}{4b_0} \right\}. \quad (48)$$

The theorem follows from Corollary 5 in [Loh and Wainwright \(2012\)](#), so long as we can show that condition (48) holds for $\lambda^{(i)} \geq 4\psi_i \sqrt{\frac{\log m}{n}}$, where the parameter ψ_i is as defined in (44). Condition (48) can be easily checked using the definition of s_0 as in (35) and the lower bound of $\lambda^{(i)}$. Hence, by Theorem 3 and Corollary 5 in [Loh and Wainwright \(2012\)](#), we have

$$\left\| \widehat{\Theta} - \Theta \right\|_2 = O_p \left(\frac{K^2(A)}{\lambda_{\min}^2(A)} d \max_i \lambda^{(i)} \right).$$

This completes the proof. \square

Appendix E: Consistency of $\widehat{\Omega}$

Theorem 4 shows the consistency of $\widehat{\Omega}$ in the operator norm. Using the similar argument presented in the proof of Theorem 1 with appropriate modifications, we can show consistency results of $\Omega = B^{-1}$.

Theorem 4. *Suppose the columns of Ω is d_Ω -sparse, and suppose the condition number $\kappa(\Omega)$ is finite. Suppose all conditions of Theorem 1 in the main paper hold by changing m and n each other, and replacing d with d_Ω . Then with probability at least $1 - 26/m^2$,*

$$\left\| \widehat{\Omega} - \Omega \right\|_2 = O_p \left(\frac{K^2(B)}{\lambda_{\min}^2(B)} d_\Omega \max_{i \leq n} \lambda^{(i)} \right).$$

Appendix F: Proof of lemmas

The large deviation bounds in Lemmas 4 and 3 are the key results in proving Lemmas 1 and 2. Let C_0 be an absolute constant appropriately chosen. We first prove Lemma 2 followed by Lemma 1.

F.1. Preliminary Results

Let Z be a Gaussian ensemble such that $Z_{jk} \sim \mathcal{N}(0, 1)$ for all j, k . First we note that for a mean zero normal random variable $V_{0,j}$ with variance $\sigma_{V_j}^2$, $V_{0,j}/\sigma_{V_j} \sim$

Z_{ij} , for which it holds that $\|Z_{ij}\|_{\psi_2} = K$. Thus we have

$$\|V_{0,j}/\sigma_{V_j}\|_{\psi_2} = K \text{ and thus } \|V_{0,j}\|_{\psi_2} = \sigma_{V_j}K =: M_{V_j}$$

which reflects the relative strength of the noise in V_0 relative to Z_{ij} and $M_V := \max_j M_{V_j} = K \max_j \sigma_{V_j}$ is the upper bound on ψ_2 norm for $V_{0,j}, j = 1, \dots, m$.

Throughout this section, we denote by:

$$r_{m,n} = C_0 K^2 \sqrt{\frac{\log m}{n}} \quad \text{and} \quad r_{m,m} = 2C_0 K^2 \sqrt{\frac{\log m}{mn}}.$$

We first define some events $\mathcal{B}_4, \mathcal{B}_5, \mathcal{B}_6, \mathcal{B}_{10}$ which are adapted from Lemmas 5 and 11 of [Rudelson and Zhou \(2017\)](#).

Denote by $\mathcal{B}_0 := \mathcal{B}_4 \cap \mathcal{B}_5 \cap \mathcal{B}_6 \cap \mathcal{B}_{10}$, which we use throughout this paper. Denote by $\bar{\beta}^j \in \mathbb{R}^m$ the zero-extended β^j in \mathbb{R}^m such that $\bar{\beta}_i^j = \beta_i^j \ \forall i \neq j$ and $\bar{\beta}_j^j = 0$.

Lemma 3. [Lemma 11 of [Rudelson and Zhou \(2017\)](#)] Assume that the stable rank of B , $\|B\|_F^2 / \|B\|_2^2 \geq \log m$. Let Z, X_0 and W as defined in Theorem 2. Let Z_0, Z_1 and Z_2 be independent copies of Z . Let $V_j^T \sim Y_j \sigma_{V_j}$ where $Y_j := e_j^T Z_0^T$. Denote by \mathcal{B}_4 the event such that

$$\begin{aligned} \text{for every } j, \quad \frac{1}{n} \left\| A^{\frac{1}{2}} Z_1^T V_j \right\|_{\infty} &\leq r_{m,n} \sigma_{V_j} a_{\max}^{1/2} \\ \text{and } \frac{1}{n} \left\| Z_2^T B^{\frac{1}{2}} V_j \right\|_{\infty} &\leq r_{m,n} \sigma_{V_j} \sqrt{\tau_B}. \end{aligned}$$

Then $\mathbb{P}(\mathcal{B}_4) \geq 1 - 4/m^2$. Moreover, denote by \mathcal{B}_5 the event such that

$$\begin{aligned} \text{for every } j, \quad \frac{1}{n} \left\| (Z^T B Z - \text{tr}(B) I_m) \bar{\beta}^j \right\|_{\infty} &\leq r_{m,n} \|\beta^j\|_2 \frac{\|B\|_F}{\sqrt{n}} \\ \text{and } \frac{1}{n} \left\| X_0^T W \bar{\beta}^j \right\|_{\infty} &\leq r_{m,n} \|\beta^j\|_2 \sqrt{\tau_B} a_{\max}^{1/2}. \end{aligned}$$

Then $\mathbb{P}(\mathcal{B}_5) \geq 1 - 4/m^2$.

Finally, denote by \mathcal{B}_{10} the event such that

$$\begin{aligned} \frac{1}{n} \left\| (Z^T B Z - \text{tr}(B) I_m) \right\|_{\max} &\leq r_{m,n} \frac{\|B\|_F}{\sqrt{n}} \\ \text{and } \frac{1}{n} \left\| X_0^T W \right\|_{\max} &\leq r_{m,n} \sqrt{\tau_B} a_{\max}^{1/2}. \end{aligned}$$

Then $\mathbb{P}(\mathcal{B}_{10}) \geq 1 - 4/m^2$.

Next we state the following result from [Rudelson and Zhou \(2017\)](#).

Lemma 4. [Lemma 5 of Rudelson and Zhou (2017)] Let $m \geq 2$. Let X be defined as in (3). Suppose that $n \vee (r(A)r(B)) > \log m$. Denote by \mathcal{B}_6 the event such that

$$|\hat{\tau}_B - \tau_B| \leq 2C_0 K^2 \sqrt{\frac{\log m}{mn}} \left(\frac{\|A\|_F}{\sqrt{m}} + \frac{\|B\|_F}{\sqrt{n}} \right) =: D_1 r_{m,m}$$

$$\text{where } D_1 := \frac{\|A\|_F}{\sqrt{m}} + \frac{\|B\|_F}{\sqrt{n}} \text{ and } r_{m,m} = 2K^2 C_0 \sqrt{\frac{\log m}{mn}}.$$

Then $\mathbb{P}(\mathcal{B}_6) \geq 1 - \frac{3}{m^3}$. If we replace $\sqrt{\log m}$ with $\log m$ in the definition of event \mathcal{B}_6 , then we can drop the condition on n or $r(A)r(B) = \frac{\text{tr}(A)}{\|A\|_2} \frac{\text{tr}(B)}{\|B\|_2}$ to achieve the same bound on event \mathcal{B}_6 .

F.2. Proof of Lemma 2

Clearly the condition on the stable rank of B guarantees that

$$n \geq r(B) = \frac{\text{tr}(B)}{\|B\|_2} = \frac{\text{tr}(B) \|B\|_2}{\|B\|_2^2} \geq \|B\|_F^2 / \|B\|_2^2 \geq \log m.$$

Thus the conditions in Lemmas 4 and 3 hold. A careful examination of the proof for Theorem 1 in Rudelson and Zhou (2017) shows that the key new component is in analyzing the following term $\hat{\gamma}^{(i)}$ for all i . First notice that for all i ,

$$n\hat{\gamma}^{(i)} = X_{-i}^T X_i = (X_{0,-i}^T + W_{-i}^T)(X_{0,-i} \beta^i + \varepsilon_i),$$

where $\varepsilon_i := V_{0,i} + W_i$, and

$$\begin{aligned} \hat{\Gamma}^{(i)} \beta^i &= \frac{1}{n} (X_{-i}^T X_{-i} - \hat{\text{tr}}(B) I_{m-1}) \beta^i \\ &= \frac{1}{n} (X_{0,-i}^T X_{0,-i} + W_{-i}^T X_{0,-i} + X_{0,-i}^T W_{-i} + W_{-i}^T W_{-i} - \hat{\text{tr}}(B) I_{m-1}) \beta^i \end{aligned}$$

Thus

$$\begin{aligned} \left\| \hat{\gamma}^{(i)} - \hat{\Gamma}^{(i)} \beta^i \right\|_\infty &\leq \frac{1}{n} \left\| X_{0,-i}^T \varepsilon_i + W_{-i}^T \varepsilon_i - (X_{0,-i}^T W_{-i} + W_{-i}^T W_{-i} - \hat{\text{tr}}(B) I_{m-1}) \beta^i \right\|_\infty \\ &\leq \frac{1}{n} \left\| X_{0,-i}^T \varepsilon_i + W_{-i}^T \varepsilon_i \right\|_\infty + \frac{1}{n} \left\| (W^T W - \hat{\text{tr}}(B) I_m) \bar{\beta}^i \right\|_\infty + \left\| \frac{1}{n} X_0^T W \bar{\beta}^i \right\|_\infty \\ &\leq \frac{1}{n} \left\| X_{0,-i}^T \varepsilon_i + W_{-i}^T \varepsilon_i \right\|_\infty + \frac{1}{n} \left\| (Z^T B Z - \text{tr}(B) I_m) \bar{\beta}^i \right\|_\infty + \frac{1}{n} \left\| X_0^T W \bar{\beta}^i \right\|_\infty \\ &\quad + \frac{1}{n} \left| \hat{\text{tr}}(B) - \text{tr}(B) \right| \left\| \beta^i \right\|_\infty =: U_1 + U_2 + U_3 + U_4. \end{aligned}$$

By Lemma 3, on event \mathcal{B}_{10} ,

$$\max_{i \neq j} \frac{1}{n} \langle X_{0,j}, W_i \rangle \leq \frac{1}{n} |X_0^T W|_{\max} \leq C_0 K^2 \sqrt{\tau_B} \sqrt{a_{\max}} \sqrt{\frac{\log m}{n}} = \sqrt{\tau_B} \sqrt{a_{\max}} r_{m,n},$$

$$\max_{i \neq j} \frac{1}{n} \langle W_i, W_j \rangle \leq C_0 K^2 \frac{1}{\sqrt{n}} \|B\|_F \sqrt{\frac{\log m}{n}} = \frac{1}{\sqrt{n}} \|B\|_F r_{m,n}.$$

On event \mathcal{B}_4 , we have for every i ,

$$\max_{j \neq i} \frac{1}{n} \langle X_{0,j}, V_{0,i} \rangle \leq C_0 K^2 \sigma_{V_i} \sqrt{a_{\max}} \sqrt{\frac{\log m}{n}} = \sigma_{V_i} r_{m,n} \sqrt{a_{\max}}$$

$$\text{and } \max_{j \neq i} \frac{1}{n} \langle W_j, V_{0,i} \rangle \leq C_0 K^2 \sigma_{V_i} \sqrt{\tau_B} \sqrt{\frac{\log m}{n}} = r_{m,n} \sigma_{V_i} \sqrt{\tau_B},$$

where C_0 is adjusted so that the error probability hold for $D_0 = \sqrt{\tau_B} + a_{\max}^{1/2}$.

On event \mathcal{B}_5 for $D'_0 := \sqrt{\|B\|_2} + a_{\max}^{1/2}$, for all j ,

$$\begin{aligned} U_2 + U_3 &= \frac{1}{n} \|(Z^T B Z - \text{tr}(B) I_m) \bar{\beta}^j\|_{\infty} + \frac{1}{n} \|X_0^T W \bar{\beta}^j\|_{\infty} \\ &\leq r_{m,n} \|\beta^j\|_2 \left(\frac{\|B\|_F}{\sqrt{n}} + \sqrt{\tau_B} a_{\max}^{1/2} \right) \leq r_{m,n} \|\beta^j\|_2 \tau_B^{1/2} D'_0, \end{aligned}$$

where recall $\|B\|_F \leq \sqrt{\text{tr}(B)} \|B\|_2^{1/2}$. Denote by $\mathcal{B}_0 := \mathcal{B}_4 \cap \mathcal{B}_5 \cap \mathcal{B}_6 \cap \mathcal{B}_{10}$.

Suppose that event \mathcal{B}_0 holds. By Lemmas 4 and 3, under (A1) and D_1 defined therein, for all i ,

$$\begin{aligned} \|\hat{\gamma}^{(i)} - \hat{\Gamma}^{(i)} \beta^i\|_{\infty} &\leq r_{m,n} \sigma_{V_i} D_0 + D'_0 \tau_B^{1/2} r_{m,n} \|\beta^i\|_2 + \frac{1}{n} |\hat{\text{tr}}(B) - \text{tr}(B)| \|\beta^i\|_{\infty} \\ &\leq D_0 \sigma_{V_i} r_{m,n} + D'_0 \tau_B^{1/2} \|\beta^i\|_2 r_{m,n} + D_1 \|\beta^i\|_{\infty} r_{m,n} \\ &\leq D_0 \sigma_{V_i} r_{m,n} + D'_0 \tau_B^{1/2} \|\beta^i\|_2 r_{m,n} + 2D_1 \frac{1}{\sqrt{m}} \|\beta^i\|_{\infty} r_{m,n} \end{aligned} \quad (49)$$

By (49) and that fact that

$$2D_1 := 2 \left(\frac{\|A\|_F}{\sqrt{m}} + \frac{\|B\|_F}{\sqrt{n}} \right) \leq 2(\|A\|_2^{1/2} + \|B\|_2^{1/2})(\sqrt{\tau_A} + \sqrt{\tau_B}) \leq D_{\text{oracle}} D'_0,$$

we have on \mathcal{B}_0 and under (A1), for all i

$$\begin{aligned} \|\hat{\gamma}^{(i)} - \hat{\Gamma}^{(i)} \beta^i\|_{\infty} &\leq D'_0 \tau_B^{1/2} \|\beta^i\|_2 r_{m,n} + 2D_1 \frac{1}{\sqrt{m}} \|\beta^i\|_{\infty} r_{m,n} + D_0 \sigma_{V_i} r_{m,n} \\ &\leq D'_0 \|\beta^i\|_2 r_{m,n} \left(\tau_B^{1/2} + \frac{D_{\text{oracle}}}{\sqrt{m}} \right) + D_0 \sigma_{V_i} r_{m,n} \\ &\leq D'_0 \left(\tau_B^{1/2} + \frac{D_{\text{oracle}}}{\sqrt{m}} \right) \|\beta^i\|_2 r_{m,n} + D_0 \sigma_{V_i} r_{m,n} \\ &\leq D'_0 \left(\tau_B^{+1/2} \|\beta^i\|_2 + \sigma_{V_i} \right) r_{m,n}. \end{aligned}$$

Hence the lemma holds for $m \geq 16$ and $\psi_i = C_0 D'_0 K^2 \left(\tau_B^{+/2} \|\beta^i\|_2 + \sigma_{V_i} \right)$. Finally, we have by the union bound, $\mathbb{P}(\mathcal{B}_0) \geq 1 - 16/m^2$. This completes the proof. \square

F.3. Proof of Lemma 1

Lemma 1 follows from the proof of Theorem 26 of Rudelson and Zhou (2017).

Hence we only provide a proof sketch.

Recall the following for $X_0 = Z_1 A^{1/2}$,

$$\begin{aligned} \Delta &:= \widehat{\Gamma}_A - A := \frac{1}{n} X^T X - \frac{1}{n} \widehat{\text{tr}}(B) I_m - A \\ &= \left(\frac{1}{n} X_0^T X_0 - A \right) + \frac{1}{n} (W^T X_0 + X_0^T W) + \frac{1}{n} (W^T W - \widehat{\text{tr}}(B) I_m). \end{aligned}$$

First notice that

$$\begin{aligned} & \left| \widehat{\Gamma}_A - A \right|_{\max} \\ & \leq \left| \frac{1}{n} X_0^T X_0 - A \right|_{\max} + \left| \frac{1}{n} (W^T X_0 + X_0^T W) \right|_{\max} + \left| \frac{1}{n} W^T W - \frac{\widehat{\text{tr}}(B)}{n} I_m \right|_{\max} \\ & \leq \left| A^{1/2} \frac{1}{n} Z_1^T Z_1 A^{1/2} - A \right|_{\max} + \left| \frac{1}{n} (W^T X_0 + X_0^T W) \right|_{\max} \\ & \quad + \left| \frac{1}{n} Z_2^T B Z_2 - \tau_B I_m \right|_{\max} + \frac{1}{n} \left| \widehat{\text{tr}}(B) - \text{tr}(B) \right|_{\max} \\ & =: I + II + III + IV. \end{aligned}$$

Denote by \mathcal{B}_{10} the event such that

$$\begin{aligned} \frac{1}{n} |X_0^T W|_{\max} & \leq C_0 K^2 \sqrt{\tau_B a_{\max}} \sqrt{\frac{\log m}{n}} \\ \left| \frac{1}{n} Z^T B Z - \text{tr}(B) I_m / n \right|_{\max} & = \frac{1}{n} |W^T W - \text{tr}(B) I_m|_{\max} \\ & \leq C_0 K^2 \frac{\|B\|_F}{\sqrt{n}} \sqrt{\frac{\log m}{n}} \leq C_0 K^2 \|B\|_2 \sqrt{\frac{\log m}{n}}. \end{aligned}$$

Then, \mathcal{B}_{10} holds with probability at least $1 - 2/m^2$. See Lemma 3 of Rudelson and Zhou (2017).

Denote by event \mathcal{B}_3 the event such that

$$\frac{1}{n} |X_0^T X_0 - A|_{\max} \leq 4C\varepsilon a_{\max},$$

where $\varepsilon = K^2 \sqrt{\frac{\log m}{n}} < 1/C$; Then $\mathbb{P}(\mathcal{B}_3) \geq 1 - 2/m^2$ so long as $n \geq c' K^4 \log(3em/\varepsilon)/\varepsilon^2$, which in turn holds so long as c' is small enough; See Corollary 42 of Rudelson and Zhou (2017).

Putting all together, we have under $\mathcal{B}_{10} \cap \mathcal{B}_3 \cap \mathcal{B}_6$

$$\left| \widehat{\Gamma}_A - A \right|_{\max} \leq 8CK^2(a_{\max} + \|B\|_2) \sqrt{\frac{\log m}{n}} + 4C_0D_1K^2 \sqrt{\frac{\log m}{mn}}.$$

This completes the proof. \square

Appendix G: R-squared analysis

Consider the following regressions as considered in (19) and (20) in the main paper:

$$\begin{aligned} y &= X\beta_1 + \epsilon, \quad X \text{ and } y \text{ are observable,} \\ y &= X_0\beta_2 + \epsilon, \quad X = X_0 + W, \quad X \text{ and } y \text{ are observable.} \end{aligned}$$

We calculate the explanatory power of X for y using $R_X^2 = \text{corr}(X\widehat{\beta}_1, y)^2$, where $\widehat{\beta}_1$ is the Lasso or the ridge regression estimator.

Similarly, define the explanatory power of X_0 for y using the EIV estimator $\widehat{\beta}_2$:

$$R_{X_0}^2 = \text{corr}(X_0\widehat{\beta}_2, y)^2 = \frac{\text{Cov}(y, X_0\widehat{\beta}_2)^2}{\text{Var}(y) \text{Var}(X_0\widehat{\beta}_2)}. \quad (50)$$

The following Lemma 5 implies that when the model follows EIV with fixed m , $R_{X_0}^2$ becomes larger than R_X^2 as n increases, i.e., the proposed R-squared metric asymptotically choose a correct model between EIV and the regular regression model.

Lemma 5. Suppose EIV model as in (1) and (3) in the main paper with $E\epsilon^2 = \sigma^2$ and $\mathbb{E}\epsilon = 0$. Suppose $X_0 = Z_1A^{1/2}$ and $W = B^{1/2}Z_2$ for independent random matrices Z_1 and Z_2 with i.i.d. $N(0, 1)$ entries, for $1 \leq i \leq j \leq m$. Let $\widehat{\beta}$ be the corrected Lasso (i.e. EIV) and $\widehat{\beta}_L$ and $\widehat{\beta}_R$ be the Lasso and the ridge regression estimator with regularization parameters λ_L and λ_R respectively, as defined in Section 4.3 of the main paper. Then as $n \rightarrow \infty$ with fixed m , $\lambda_L \rightarrow 0$, and $\lambda_R/n \rightarrow 0$, it holds that $R_{X_0}^2 - R_X^2 \rightarrow c$ in probability for some $c > 0$; c depends only on A , B , β_2 , and σ^2 .

Proof. Throughout the proof, for a sequence of numbers $\{a_n\}_{n \geq 1}$ and a number b , we use $a_n \xrightarrow{P} b$ when a_n converges to b in probability. For a sequence of matrices $\{\Sigma_n\}_{n \geq 1}$ and a matrix Σ , we use $\Sigma_n \xrightarrow{P} \Sigma$ when every element of Σ_n

converges to the corresponding element of Σ in probability, which implies that $\|\Sigma_n - \Sigma\|_F \xrightarrow{P} 0$. Note that

$$\tilde{\beta}_L = \arg \min_{\beta \in \mathbb{R}^m} \frac{1}{2n} \beta^T X^T X \beta - \frac{1}{n} y^T X \beta + \lambda \|\beta\|_1 := \arg \min_{\beta \in \mathbb{R}^m} g_n(\beta).$$

Since $X_0 = Z_1 A^{1/2}$ and $W = B^{1/2} Z_2$ for random matrices Z_1 and Z_2 having i.i.d. $N(0, 1)$ entries, for $1 \leq i \leq j \leq m$,

$$\frac{1}{n} X^T X \xrightarrow{P} A + \tau_B I_m \quad \text{and} \quad \frac{1}{n} y^T X \xrightarrow{P} \beta_2^T A.$$

Combining the above with $\lambda \rightarrow 0$,

$$g_n(\beta) \xrightarrow{P} g(\beta) := \frac{1}{2} \beta^T (A + \tau_B I_m) \beta - \beta_2^T A \beta.$$

Since $g_n(\beta)$ is convex, it follows from [Knight and Fu \(2000\)](#) that

$$\arg \min_{\beta \in \mathbb{R}^m} g_n(\beta) \xrightarrow{P} \arg \min_{\beta \in \mathbb{R}^m} g(\beta).$$

Hence $\tilde{\beta}_L \xrightarrow{P} (A + \tau_B I_m)^{-1} A \beta_2$.

Note that

$$\tilde{\beta}_R = (X^T X + \lambda_R I_p)^{-1} X^T y = \left(\frac{X^T X}{n} + \frac{\lambda_R}{n} I_m \right)^{-1} \frac{X^T y}{n}.$$

Since $\frac{X^T X}{n} \xrightarrow{P} A + \tau_B I_m$, $\frac{\lambda_R}{n} \rightarrow 0$, and $\frac{X^T y}{n} \xrightarrow{P} A \beta_2$, we have

$$\tilde{\beta}_R \xrightarrow{P} (A + \tau_B I_m)^{-1} A \beta_2.$$

Since it holds that

$$\begin{aligned} \text{Var}(y) &\xrightarrow{P} \sigma^2 + \beta_2^T A \beta_2 \quad \text{and} \\ \text{Var}(X \tilde{\beta}_R), \text{Cov}(y, X \tilde{\beta}_R) &\xrightarrow{P} \beta_2^T A (A + \tau_B I_m)^{-1} A \beta_2, \end{aligned}$$

and

$$\text{Var}(X_0 \hat{\beta}), \text{Cov}(y, X_0 \hat{\beta}) \xrightarrow{P} \beta_2^T A \beta_2,$$

we have

$$R_X^2 = \frac{\text{Cov}(y, X \tilde{\beta}_R)^2}{\text{Var}(y) \text{Var}(X \tilde{\beta}_R)} \xrightarrow{P} \frac{\beta_2^T A (A + \tau_B I_m)^{-1} A \beta_2}{\beta_2^T A \beta_2 + \sigma^2} := \tilde{r}^*,$$

and

$$R_{X_0}^2 = \frac{\text{Cov}(y, X_0 \hat{\beta})^2}{\text{Var}(y) \text{Var}(X_0 \hat{\beta})} \xrightarrow{\text{P}} \frac{\beta_2^T A \beta_2}{\beta_2^T A \beta_2 + \sigma^2} := r^*.$$

Therefore,

$$\begin{aligned} (r^* - \tilde{r}^*)(\beta_2^T A \beta_2 + \sigma^2) &= \beta_2^T (A - A(A + \tau_B I_m)^{-1} A) \beta_2 \\ &\geq \|\beta_2\|_2^2 \frac{\lambda_{\min}(A) \tau_B}{\lambda_{\min}(A) + \tau_B}, \end{aligned}$$

where the last inequality follows from the fact that $A - A(A + \tau_B I_m)^{-1} A$ is positive definite since it has positive eigenvalues $\frac{\lambda_i(A) \tau_B}{\lambda_i(A) + \tau_B} (i = 1, \dots, m)$. This completes the proof. \square

In practice, $R_{X_0}^2$ defined in (50) should be estimated since X_0 is not observed. Under the setting in Theorem 1 in the main paper, we obtain a lower bound of $R_{X_0}^2$ by the function of $\hat{\beta}$, \hat{A}_+ , and \hat{B}_+ , where $\hat{A}_+ := \hat{\Theta}_+^{-1}$ and $\hat{B}_+ := \hat{\Omega}_+^{-1}$.

Consider the subgaussian model (3). Then, we have with high probability

$$\begin{aligned} \text{Var}(X_0 \hat{\beta}_2) &= \hat{\beta}_2^T \left(\frac{X_0^T X_0}{n} - \frac{X_0^T 1_n 1_n^T X_0}{n^2} \right) \hat{\beta}_2 \\ &= \hat{\beta}_2^T A^{1/2} \left(\frac{Z_1^T Z_1}{n} - \frac{Z_1^T 1_n 1_n^T Z_1}{n^2} \right) A^{1/2} \hat{\beta}_2 \\ &\leq \lambda_{\max}(A) \lambda_{\max}(Z_1^T Z_1 / n) \|\hat{\beta}_2\|^2 \\ &\leq \left(1 + \frac{m \log n}{4n} \right) \lambda_{\max}(A) \|\hat{\beta}_2\|^2 \\ &\leq 2 \left(1 + \frac{m \log n}{4n} \right) \lambda_{\max}(\hat{A}_+) \|\hat{\beta}_2\|^2 \end{aligned} \tag{51}$$

where the first inequality uses $\|I_n - 1_n 1_n^T / n\|_2 \leq 1$, the second inequality follows from Lemma 6, and the last inequality uses the fact that $\lambda_{\max}(A) \leq 2\lambda_{\max}(\hat{A}_+)$, which holds with high probability; with regard to the last claim, see the proof of Theorem 1.

When $1_n^T y = 0$, the numerator of (50) is

$$\text{Cov}(y, X_0 \hat{\beta}_2)^2 = \left(\frac{1}{n} \hat{\beta}_2^T X_0^T y \right)^2.$$

Thus we have with probability $1 - 2n^{-\frac{cm}{8K^2}}$,

$$\begin{aligned}
& \frac{1}{n} \widehat{\beta}_2^T X_0^T y = \frac{1}{n} \widehat{\beta}_2^T X^T y - \frac{1}{n} \widehat{\beta}_2^T W^T y = \frac{1}{n} \widehat{\beta}_2^T X^T y - \frac{1}{n} \widehat{\beta}_2^T Z_2^T B^{1/2} y \quad (52) \\
& \geq \frac{1}{n} \widehat{\beta}_2^T X^T y - \frac{1}{n} \|\widehat{\beta}_2\|_2 \|Z_2^T B^{1/2} y\|_2 \\
& \geq \frac{1}{n} \widehat{\beta}_2^T X^T y - \frac{1}{\sqrt{n}} \sqrt{1 + \frac{m \log n}{4n}} \|\widehat{\beta}_2\|_2 \|y\|_2 \|B\|_2^{1/2} \\
& \geq \frac{1}{n} \widehat{\beta}_2^T X^T y - \frac{\sqrt{2}}{\sqrt{n}} \sqrt{1 + \frac{m \log n}{4n}} \|\widehat{\beta}_2\|_2 \|y\|_2 \|\widehat{B}_+\|_2^{1/2},
\end{aligned}$$

where we use Lemma 6 and Theorem 1 in the main paper. Hence, we obtain a lower bound of $\text{Cov}(y, X_0 \widehat{\beta}_2)^2$. Together with (51), we obtain a lower bound of $R_{X_0}^2$, as expressed in (22) in the main paper.

Lemma 6. *Let Z be an $n \times m$ random matrix with independent entries Z_{ij} satisfying $E(Z_{ij}) = 0$, $E(Z_{ij}^2) = 1$, and $\|Z_{ij}\|_{\psi_2} \leq K$. Suppose for the absolute constant $c > 0$ defined in (53), the following holds:*

$$\frac{4n}{m \log n} \vee 32 \left(\sqrt{\frac{m}{n}} + \frac{m}{n} \right) \frac{n}{m \log n} \leq \frac{1}{3} n^{\frac{c}{8K^2}}.$$

Then, we have with probability at least $1 - 2n^{-\frac{cm}{8K^2}}$, $\|\frac{1}{n} Z^T Z\|_2 \leq 1 + \frac{m \log n}{4n}$.

Proof. By Theorem 31 of Rudelson and Zhou (2017), we have for any $u \in S^{m-1}$ and $t > 0$,

$$P \left(\left| u^T \frac{Z^T Z}{n} u - 1 \right| > t \right) \leq 2 \exp \left(-c \min \left(\frac{nt^2}{K^4}, \frac{nt}{K^2} \right) \right).$$

Consider the ϵ -net of S^{m-1} . Let S_ϵ be the set of centers of the ϵ -net. Then, there exists an absolute constant $c > 0$ such that for $t > K^2$,

$$P \left(\exists u \in S_\epsilon \mid \left| u^T \frac{Z^T Z}{n} u - 1 \right| > t \right) \leq 2 \exp \left(m \log(3/\epsilon) - c \frac{nt}{K^2} \right). \quad (53)$$

Set $\epsilon = n^{-c_1}$ and $t = \frac{m \log n}{4n}$, where $c_1 > 0$ satisfies

$$\frac{4n}{m \log n} \vee 32 \left(\sqrt{\frac{m}{n}} + \frac{m}{n} \right) \frac{n}{m \log n} \leq n^{c_1} \leq \frac{1}{3} n^{\frac{c}{8K^2}}.$$

Then, we have

$$P \left(\left\| \frac{1}{n} Z^T Z - I_m \right\|_2 \geq \frac{m \log n}{4n} \right) \geq 1 - 2n^{-\frac{cm}{8K^2}}.$$

This completes the proof. \square

Appendix H: Additional Real Data Analysis

In this section, we include the additional real data analysis.

H.1. R -squared analysis

Figure 7 displays the R -squared values by varying regularization parameters. It is observed that EIV always has larger maximum R^* values than maximum R -squared values of Lasso and Ridge. Considering the fact that R^* is a lower bound of R -squared value of EIV, the relations of the torque data \tilde{X} and the neural signal difference Δ is well explained by EIV regression than regular regression.

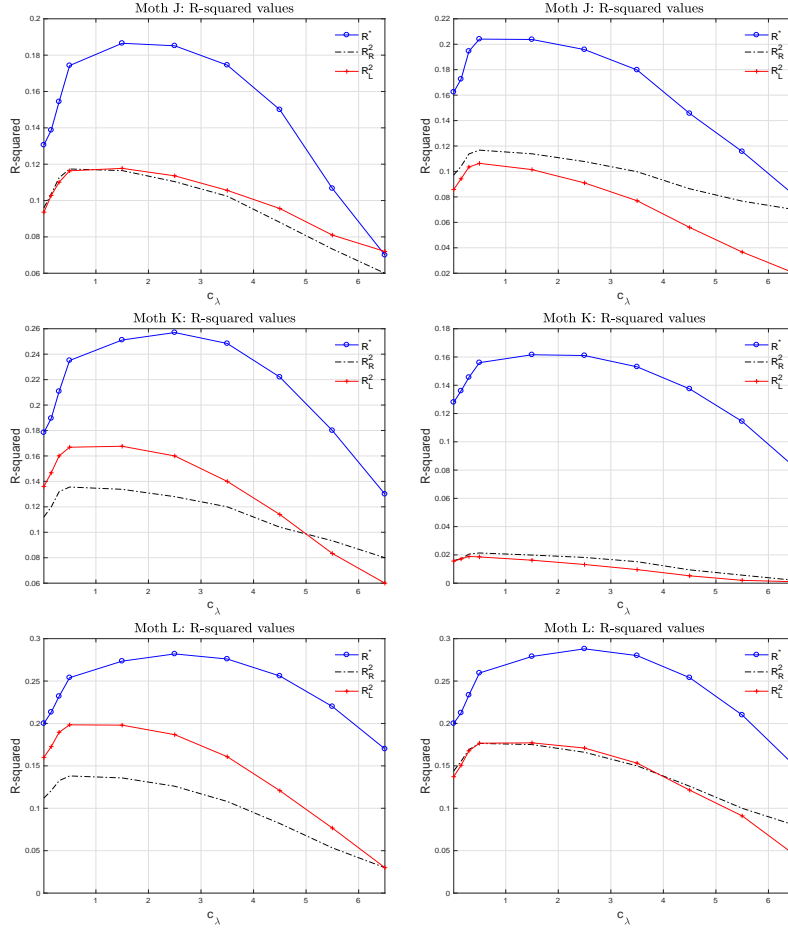


FIGURE 7. R -squared values (Lasso and Ridge) and R^* (EIV) values by varying regularization parameters. For the EIV, we set optimal $\hat{\tau}_A$ as in Table 2 in the main paper.

H.2. Supplementary of Regression Analysis

Recall that in Subsection 5.3 of the main paper, we fit regression models including EIV regression relating the residualized neural spike time differences and torque values:

$$\tilde{\Delta} = \tilde{X}\Pi\zeta_1 + \epsilon, \quad \tilde{X}\Pi \text{ and } \tilde{\Delta} \text{ are observable,} \quad (54)$$

$$\tilde{\Delta} = X_0\Pi\zeta_2 + \epsilon, \quad \tilde{X}\Pi = X_0\Pi + W\Pi, \quad \tilde{X}\Pi \text{ and } \tilde{\Delta} \text{ are observable.} \quad (55)$$

Suppose the model (54). More specifically, let $E[\tilde{X}] = 0$ and $\text{Cov}(\text{vec}\{\tilde{X}\}) = \Sigma \otimes I$. Since $\text{vec}\{\tilde{X}\Pi\} = (\Pi^T \otimes I)\text{vec}\{\tilde{X}\}$, we have

$$\begin{aligned} \text{Cov}(\text{vec}\{\tilde{X}\Pi\}) &= (\Pi^T \otimes I)E[\text{vec}(\tilde{X})\text{vec}(\tilde{X})^T](\Pi \otimes I) \\ &= (\Pi^T \otimes I)(\Sigma \otimes I)(\Pi \otimes I) \\ &= \Pi^T \Sigma \Pi \otimes I, \end{aligned}$$

that is, (54) also follows the regular linear model.

Suppose the model (55). We will show that $\tilde{X}\Pi$ in (55) has the Kronecker sum covariance structure, i.e., (55) still follows EIV model. Since $E[\tilde{X}] = 0$ and $\text{Cov}(\text{vec}(\tilde{X})) = A \oplus B$, by using the similar argument in the above with $\Pi^T \Pi = I$, we have

$$\begin{aligned} \text{Cov}(\text{vec}\{\tilde{X}\Pi\}) &= (\Pi^T \otimes I)E[\text{vec}(\tilde{X})\text{vec}(\tilde{X})^T](\Pi \otimes I) \\ &= (\Pi^T \otimes I)(A \otimes I + I \otimes B)(\Pi \otimes I) \\ &= \Pi^T A \Pi \otimes I + \Pi^T \Pi \otimes B \\ &= \Pi^T A \Pi \oplus B. \end{aligned}$$

Appendix I: Additional Tables and Figures

Figures 8-9 show the graphical structure of $\hat{\Omega}$ for moth J and L for the Kronecker sum model. Figure 10 shows heat maps of the sample correlation matrix of 500 temporal points and the sample correlation matrix of wing strokes, showing dependencies in both time points and among the wing strokes. These figures are referenced in Section 5 of the main paper.

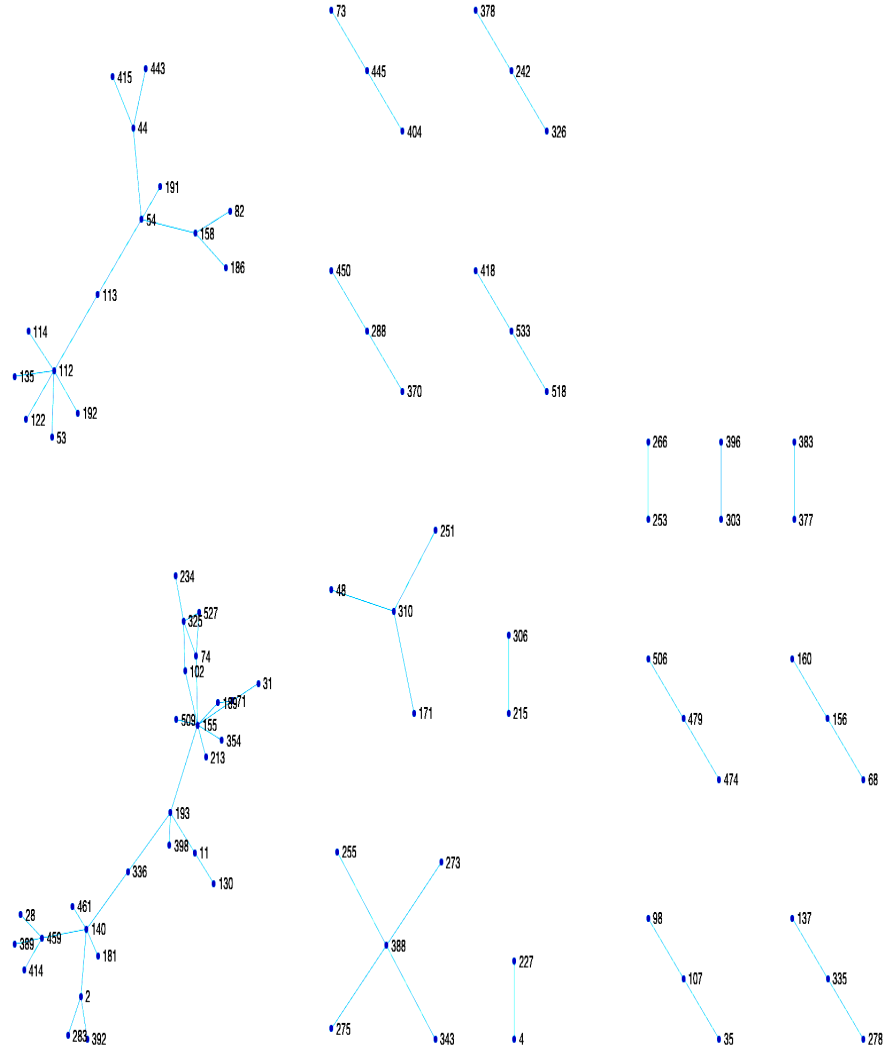


FIGURE 8. The estimated graphical structure of Ω for Moth J for the Kronecker sum model when $\hat{\tau}_A = 1.5$ and $\lambda_B^{(i)} = 0.1\sqrt{\frac{\log n}{500}} \asymp 0.01$. Singletons (nodes with edges) are not included in the graph.

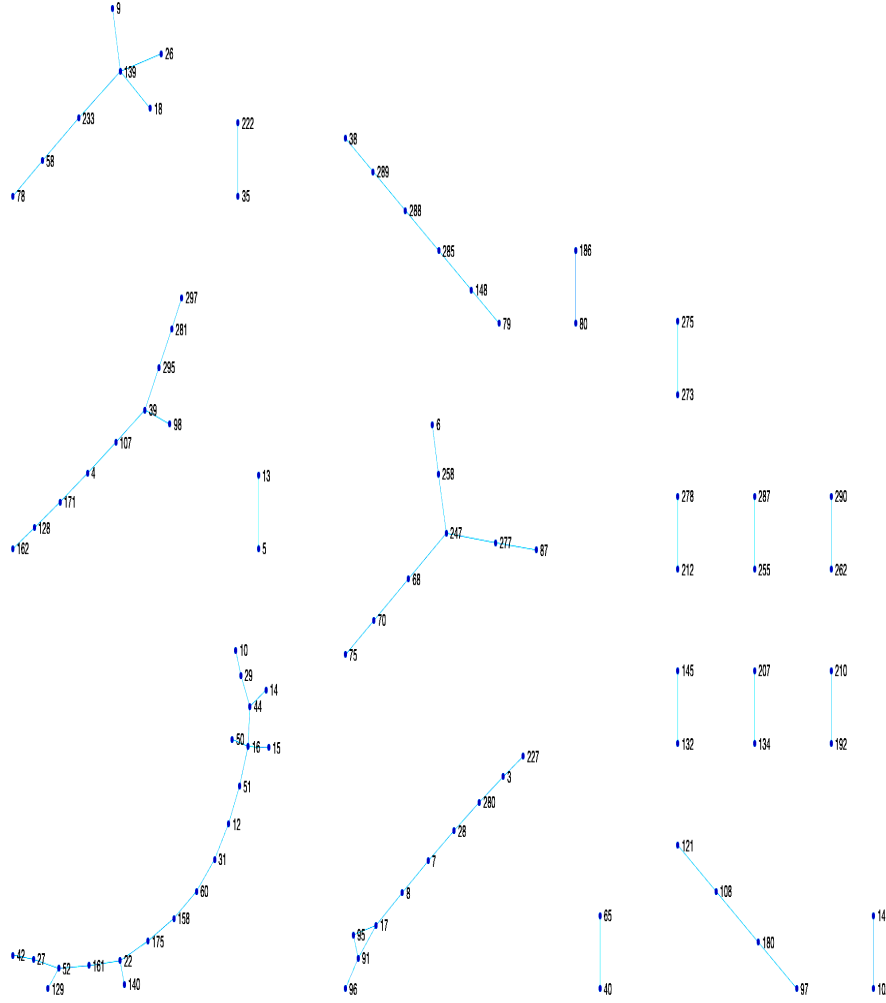


FIGURE 9. The estimated graphical structure of Ω for Moth L for the Kronecker sum model when $\hat{\tau}_A = 1.5$ and $\lambda_B^{(i)} = 0.1\sqrt{\frac{\log n}{500}} \asymp 0.01$. Nodes that have no connected edges are not included in the graph.

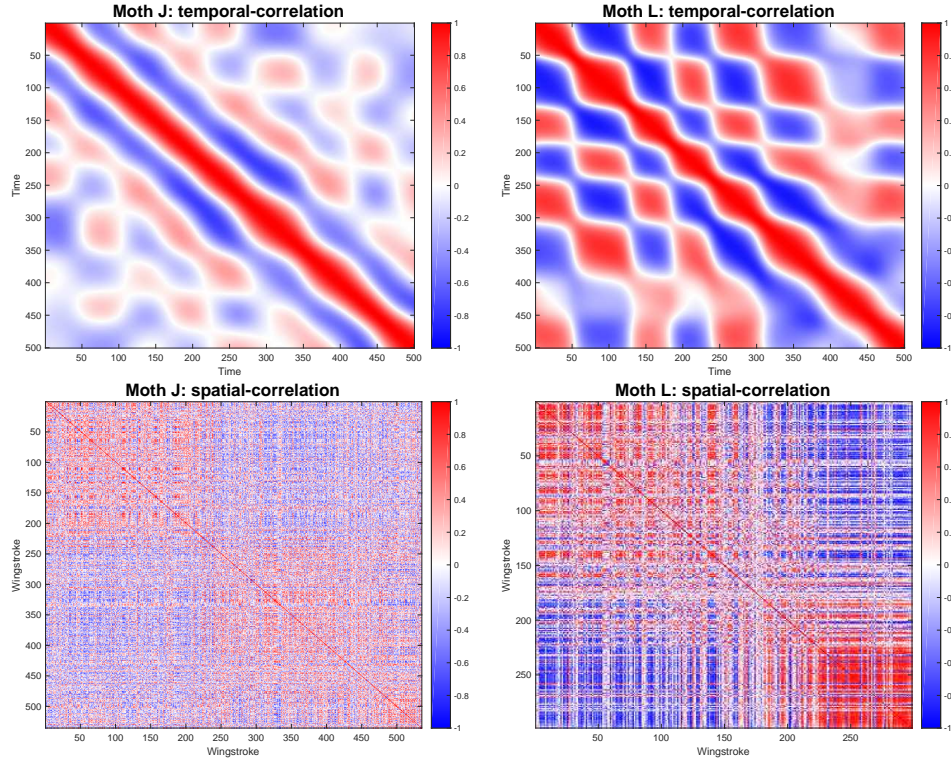


FIGURE 10. Heat maps of the sample correlation matrix of 500 temporal points (top) and the sample correlation matrix of wingstrokes (bottom) for moth J (left) and moth L (right).

References

- AGARWAL, A., NEGAHBAN, S. and WAINWRIGHT, M. (2012). Fast global convergence of gradient methods for high-dimensional statistical recovery. *Annals of Statistics* **40** 2452–2482.
- ALLEN, G. and TIBSHIRANI, R. (2010). Transposable regularized covariance models with an application to missing data imputation. *Annals of Applied Statistics* **4** 764–790.
- BELLONI, A., ROSENBAUM, M. and TSYBAKOV, A. (2016). Linear and conic programming estimators in high-dimensional errors-in-variables models. *Journal of the Royal Statistical Society, Series B* **79** 939–956.
- BONILLA, E., CHAI, K. and WILLIAMS, C. (2008). Multi-task gaussian process prediction. In *Advances in Neural Information Processing Systems 20 (NIPS 2010)*.

- CARROLL, R., RUPPERT, D., STEFANSKI, L. and CRAINICEANU, C. M. (2006). *Measurement Error in Nonlinear Models (Second Edition)*. Chapman & Hall.
- CHEN, S., DONOHO, D. and SAUNDERS, M. (1998). Atomic decomposition by basis pursuit. *SIAM Journal on Scientific and Statistical Computing* **20** 33–61.
- CHEN, Y. and CARAMANIS, C. (2013). Noisy and missing data regression: Distribution-oblivious support recovery. In *Proceedings of The 30th International Conference on Machine Learning ICML-13*.
- DUTILLEUL, P. (1999). The mle algorithm for the matrix normal distribution. *Journal of Statistical Computation and Simulation* **64** 105–123.
- EFRON, B. (2009). Are a set of microarrays independent of each other? *Annals of Applied Statistics* **3** 922–942.
- FRIEDMAN, J., HASTIE, T. and TIBSHIRANI, R. (2008). Sparse inverse covariance estimation with the graphical Lasso. *Biostatistics* **9** 432–441.
- HORNSTEIN, M., SHEDDEN, K. and ZHOU, S. (2016). Joint mean and covariance estimation with unreplicated matrix-variate data. <https://arxiv.org/abs/1611.04208>.
- KALAITZIS, A., LAFFERTY, J., LAWRENCE, N. and ZHOU, S. (2013). The bigraphical lasso. In *Proceedings of The 30th International Conference on Machine Learning ICML-13*.
- KNIGHT, K. and FU, W. (2000). Asymptotics for lasso type estimators. *The Annals of Statistics* **28** 1356–1378.
- LENG, C. and TANG, C. (2012). Sparse matrix graphical models. *Journal of American Statistical Association* **107** 1187–1200.
- LOH, P. and WAINWRIGHT, M. (2012). High-dimensional regression with noisy and missing data: Provable guarantees with nonconvexity. *Annals of Statistics* **40** 1637–1664.
- MEINSHAUSEN, N. and BÜHLMANN, P. (2006). High dimensional graphs and variable selection with the Lasso. *Annals of Statistics* **34** 1436–1462.
- ROSENBAUM, M. and TSYBAKOV, A. (2010). Sparse recovery under matrix uncertainty. *Annals of Statistics* **38** 2620–2651.
- ROSENBAUM, M. and TSYBAKOV, A. (2013). Improved matrix uncertainty selector. *IMS Collections* **9** 276–290.
- RUDELSON, M. and ZHOU, S. (2017). Errors-in-variables models with dependent measurements. *Electronic Journal of Statistics* **11** 1699–1797.

- SMITH, R., KOLENIKOV, S. and COX, L. (2003). Spatiotemporal modeling of $\text{PM}_{2.5}$ data with missing values. *Journal of Geophysical Research* **108**.
- SØRESEN, Ø., FRIGENSSI, A. and THORESEN, M. (2015). Measurement error in Lasso: Impact and likelihood bias correction. *Statistical Sinica* **25** 809–829.
- SPONBERG, S., DANIEL, T. and FAIRHALL, A. (2015). Dual dimensionality reduction reveals independent encoding of motor features in a muscle synergy for insect flight control. *PLoS Computational Biology* **11**.
- SPONBERG, S. and DANIEL, T. L. (2012). Abdicating power for control: a precision timing strategy to modulate function of flight power muscles. *Proc. R. Soc. B.* **279** 3958–3966.
- TIBSHIRANI, R. (1996). Regression shrinkage and selection via the Lasso. *Journal of the Royal Statistical Society, Series B.* **58** 267–288.
- TSILIGKARIDIS, T., HERO, A. and ZHOU, S. (2013). On convergence of kronecker graphical lasso algorithms. *IEEE Transactions on Signal Processing* **61** 1743 – 1755.
- WERNER, K., JANSSON, M. and STOICA, P. (2008). On estimation of covariance matrices with kronecker product structure. *IEEE Transactions on Signal Processing* **56** 478 – 491.
- YU, K., LAFFERTY, J., ZHU, S. and GONG, Y. (2009). Large-scale collaborative prediction using a nonparametric random effects model. *Proceedings of the 26th International Conference on Machine Learning* 1185–1192.
- YUAN, M. (2010). High dimensional inverse covariance matrix estimation via linear programming. *Journal of Machine Learning Research* **11** 2261–2286.
- ZHOU, S. (2014). Gemini: Graph estimation with matrix variate normal instances. *Annals of Statistics* **42** 532–562.
- ZHOU, S., RÜTIMANN, P., XU, M. and BÜHLMANN, P. (2011). High-dimensional covariance estimation based on Gaussian graphical models. *Journal of Machine Learning Research* **12** 2975–3026.